NEARSHORE HYDRODYNAMICS AT KAANAPALI, MAUI
&
HAWAII EXTREME WAVE STATISTICS

A THESIS SUBMITTED TO THE GRADUATE DIVISION OF THE

UNIVERSITY OF HAWAI‘I IN PARTIAL FULFILLMENT

OF THE REQUIREMENTS FOR THE DEGREE OF

MASTER OF SCIENCE

IN

GEOLOGY & GEOPHYSICS

OCTOBER 2007

By
Sean Vitousek

Thesis Committee:

Chip Fletcher, Chairperson
Mark Merrifield
Geno Pawlak
Robert Dunn

We certify that we have read this thesis and that, in our opinion, it is satisfactory in scope and quality as a thesis for the degree of Master of Science in Geology & Geophysics.

THESIS COMMITTEE

Chairperson

Table of Contents: **Page**

LIST OF TABLES ..... **iv**

LIST OF FIGURES ..... **v**

LIST OF FIGURES ..... **v**

PREFACE ..... **vii**

MODEL SCENARIOS OF SHORELINE CHANGE AT KAANAPALI BEACH MAUI, HAWAI'I **1**

ABSTRACT 1
INTRODUCTION 1
Kaanapali 2
Erosion Event 3
Seasonal Change 6
METHODS 8
Data 8
Modeling 9
COMPUTATIONAL GRIDS 10
BOUNDARY CONDITIONS 13
RESULTS 15
DISCUSSION 25
CONCLUSIONS 31
FUTURE WORK 32
ACKNOWLEDGMENTS 32
REFERENCES 33

MAXIMUM ANNUALLY RECURRING WAVE HEIGHTS IN HAWAI'I **36**

ABSTRACT 36
PREVIOUS WORK 38
MATERIALS AND METHODS 40
RESULTS 43
Log-normal and Extremal Models 43
Generalized Extreme Value (GEV) Model 47
RECOVERING SWELL DIRECTIONALITY FROM MODEL HINDCASTS 48
SIGNIFICANT WAVE HEIGHT VS. MAXIMUM PROBABLE WAVE HEIGHT 51
DISCUSSION 54
FUTURE WORK 57
ACKNOWLEDGEMENTS 58
REFERENCES 58

LIST OF TABLES

Table 1 - Model Parameters 12
Table 2 - Observed vs. modeled tidal constituents at instrument locations 16
Table 3 - The observed and modeled directional annually recurring maximum significant wave heights using extremal and GEV exceedance probability models. Wave hindcasts of Buoy 3 do not return more than one swell event per year in the southerly and westerly directional windows; hence Buoy 1 is used instead 49

LIST OF FIGURES

Figure 1 –Hawaiian Islands, Maui Nui, and Kaanapali. 2
Figure 2 - Erosion event July 2003 at Hanakao'o Point. 3
Figure 3 - Satellite altimetry map of sea surface height (SSH) in July 2003. Note the presence of the large eddy NW of the Hawaiian Islands. 4
Figure 4 - Sea-level record from Kahului, Maui. 5
Figure 5 - Wave heights in 2003 (red) compared with typical seasonal cycle of wave heights (1990-2005). 6
Figure 6 - Seasonal beach profile changes at Kaanapali Beach. 7
Figure 7 - West Maui instrument deployments in 2003. 9
Figure 8 - Instrument locations and grid layout for West Maui model. 11
Figure 9 - Nearshore grid and bathymetry for model of Kaanapali. 12
Figure 10 - Setup of boundary conditions. 13
Figure 11 - SWAN nesting scheme. WaveWatch III hindcast locations are shown in boxes. 15
Figure 12 - Modeled vs. observed current comparison for Honokowai station. 17
Figure 13 - Modeled vs. observed current comparison for the South Kahana (Airport) station. 17
Figure 14 - WaveWatch III boundary conditions and comparisons of modeled (x) and observed (-) wave heights [m] at instrument locations. The lines on the second subplot represent the south swell window (170-210^{o}). 19
Figure 15 – Wave fields (wave height in [m]) at Kaanapali based on a South swell (Hs = 1.5 m) and a north swell (Hs = 7). Significant island blockage reduces the wave height at Kaanapali due to the north swell. 20
Figure 16 – Mean wave generated currents [m/s] for South and North swell at Kaanapali Beach. 21
Figure 17 - Longshore Sediment transport patterns at Kaanapali. Tracked using a flagged patch of sand (in red - initial). Colormap represents fraction of flagged vs. unflagged sediment. 22
Figure 18 – Observed and simulated beach states during summer (left) and winter (right) swell conditions. 23
Figure 19 - Modeled longshore transport at Kaanapali for a real-time simulation summer 2003 (the year of the mesoscale eddy event). 24
Figure 20 - Computed (x) vs. observed (red) beach profile evolution for the summer of 2000. 24
Figure 21 - Relationship between the vertical components of the winds and mean flow through the Pailolo Channel recorded in the South Kahana (Airport) station. 26
Figure 22 - Observed vs. modeled beach profile changes over 3 months at a number of locations at Kaanapali, Summer 2000. 29
Figure 23 - Illustration of problems resolving small sea level changes in discrete grid based models. 30
Figure 24 - Hawaii dominant swell regimes after Moberly and Chamberlain (1964), and wave monitoring buoy locations. 39
Figure 25 - Log-normal and extremal probability models for the top 70 largest wave height events per year recorded by buoy 1. In these models the largest event (a 12.3 m

significant wave height) outlier has been removed and the peak over threshold method is used with a threshold of 5 m. 44
Figure 26 - The Generalized Extreme Value probability model used to determine the annually recurring significant wave height. 48
Figure 27 – The observed directional annually recurring maximum significant wave heights (H_s) given from extremal (A) and GEV (B) models. 49
Figure 28 - Top percent of waves vs. relation to significant wave height (H_s) 52
Figure 29 - Sensitivity of models to number of largest events selected per year. 54
Figure 30 – When a large number of events is used in analysis, the log-normal model is fit strongly the high frequency events (which represent the bulk of the data) at the expense of the extreme events. 55

PREFACE

My Masters of Science project at the University of Hawai´i involves modeling multiple coastal hazards with the end-goal to improve the scientific basis for coastal management. My advisor, Chip Fletcher, and I have focused on coastal erosion and inundation hazards as influenced by wave climates and sea-level rise. Our primary efforts involve a numerical modeling case study of beach erosion at Kaanapali, Maui, Hawai´i and with secondary efforts on determining probabilistic estimates of recurring wave heights and water levels in Hawai´i, and producing a practical means of mapping coastal inundation hazard zones.

Our case study of Kaanapali Beach focuses on the dramatic beach change in 2003 as a result of the combined effect of extreme sea levels caused by the presence of an oceanic mesoscale eddy and seasonal wave cycles. Using Delft3D, a process-based numerical model, we were able to simulate hydrodynamics, waves and sediment transport at Kaanapali. We have achieved very successful hydrodynamic and wave modeling which compares well with an extensive data set of observations along West Maui and Kaanapali collected as part of the USGS coral reef project. Sediment transport and beach morphology modeling remains the major challenge of modeling efforts. One staggering deficiency of most coastal modeling packages is the inability to resolve wave runup, and swash transport, which may significantly influence subaerial beach morphology on steep, reflective beaches such as Kaanapali.

The second aspect of this project has concerned the determination of recurring wave heights and water levels in Hawai´i. One particular focus has been on the annually recurring

wave height around the Hawaiian Island to inform the Hawai´i administrative process as to the "upper reach of the wash of the waves" which delineates the shoreline (Hawai´i Revised Statuses (H.R.S.) § 205-A). Using log-normal and extremal exceedance probability models and Generalized Extreme Value (GEV) analysis using 25 years of buoy data and long-term wave hindcasts, the annual recurring significant wave height is found to be 7.7 ± 0.2 m (25 ft ± 0.7 ft). Directional annual wave heights are also determined by applying hindcasted swell direction to observed buoy data lacking directional information.

The efforts discussed above have resulted in the following publications and conference presentations:

Vitousek, S., Fletcher, C.H., Merrifield, M.A., Pawlak, G., "Shoreline change in response to extreme tides and along-shore forcing modeled by Delft3D". *Shoreline Change Conference II Oral Presentation*. Charleston, South Carolina, May 2006.

Vitousek, S., Fletcher, C.H., Strolazzi, C.D., "Modeling alongshore propagating tides and currents at West Maui, Hawai´i: Implications for transport using Delft3D". *Poster*. AGU fall meeting. San Francisco, California, December 2006.

Vitousek, S., Fletcher, C.H., Merrifield, M.A., Pawlak, G., Storlazzi, C.D., "Model scenarios of shoreline change at Kaanapali Beach, Maui, Hawai´i: Seasonal and extreme events". *ASCE Coastal Sediments 2007 Meeting Proceedings*, v. 2, p. 1227-1240.

Vitousek, S., Fletcher, C.H., "Hawai´i Swell Record Statistics and the Maximum Annually Recurring Wave Height". *Pacific Science* (in revision)

Recently we have developed a practical/ engineering approach to mapping coastal inundation hazard zones, by applying statistical models of recurring wave heights and water levels to produce expected runup levels and return periods. These levels are mapped on high-resolution coastal elevation models produced from topographic and bathymetric LIDAR. The evolution of these inundation levels as a function of future sea-level rise is a very interesting aspect that this practical model is capable of evaluating. The major issues that question the validity of this approach are the applicability of the empirical runup equation (Stockdon et. al. 2006) and nearshore wave model (SWAN), which are used to translate the recurrence model of deep-water wave height to a recurrence model of runup. Runup remains a process that is highly variable, often unpredictable with traditional methods especially in diverse coastal environments (particularly fringing reefs) such as those found in Hawai´i. The best/most illuminating approach to study and predict runup, be it practical through empirical equations, theoretical through equations and observations of nearshore energy transfer, numerical through the use of process-based models, or a combination of these approaches remains to be seen. This is a potential topic of study for my Ph. D.

Sean Vitousek
7-31-07

MODEL SCENARIOS OF SHORELINE CHANGE AT KAANAPALI BEACH MAUI, HAWAI‘I

ABSTRACT

Kaanapali beach is a well-defined littoral cell of carbonate sand extending 2 km south from Black Rock (a basalt headland) to Hanakao'o Point. The beach experiences dynamic seasonal shoreline change forced by longshore transport from two dominant swell regimes. In summer, south swells (H_s = 1-2 m T_p = 14-25 s) drive sand to the north, while in winter, north swells (H_s = 5-8 m T_p = 14-20 s) drive sand to the south where it accumulates on a submerged fossil reef. The Delft3D modeling system accurately predicts directly observed tidal currents and wave heights around West Maui, and is applied to simulate shoreline change. Morphologic simulations qualitatively resolve the observed seasonal behavior. Quantitative comparisons of observed vs. modeled beach profile changes and potential influences of sea-level rise reveal limitations of the model.

INTRODUCTION

Numerical modeling allows for simulations of coastal behavior. The model skill, or predictive ability, may be quite good provided that physical processes involved in sediment transport and morphologic development are well resolved mathematically. Models are often criticized as "black boxes", and disconnected from reality. Thus the effort is needed to observe and, through modeling, reproduce wave and current fields with adequate spatial resolution.

The Delft3D modeling system accurately reproduces hydrodynamic behavior at a number of field sites (Elias et al. 2000; Klein et al. 2001; Luijendijk 2001; Walstra et al. 2001, 2003). Delft3D also reproduces observed sediment transport patterns in laboratory

tests and morphologic simulations (Lesser 2000; Lesser et. al. 2004; Elias 2006) using the Van Rijn 1993 transport formulations. As an extension of these successes, it is hoped that adequate resolution of water levels, waves, and currents allow the model to reproduce sediment transport patterns in carbonate reef environments.

Kaanapali

Kaanapali Beach, located on the west coast of Maui, Hawaii, lies within a well-defined littoral cell extending 2 km south from Black Rock (a basalt headland) to Hanakao'o Point. Kaanapali Beach is at the center of the Maui Nui complex shown in **Figure 1**, which consists of the islands of Molokai, Lanai, Maui, and Kahoolawe. Shadowed by these islands, Kaanapali is exposed to direct swell from limited windows: north (350-10^{o}), south (210-170^{o}), west (280-260^{o}), as well as refracted swell from the remaining directions.

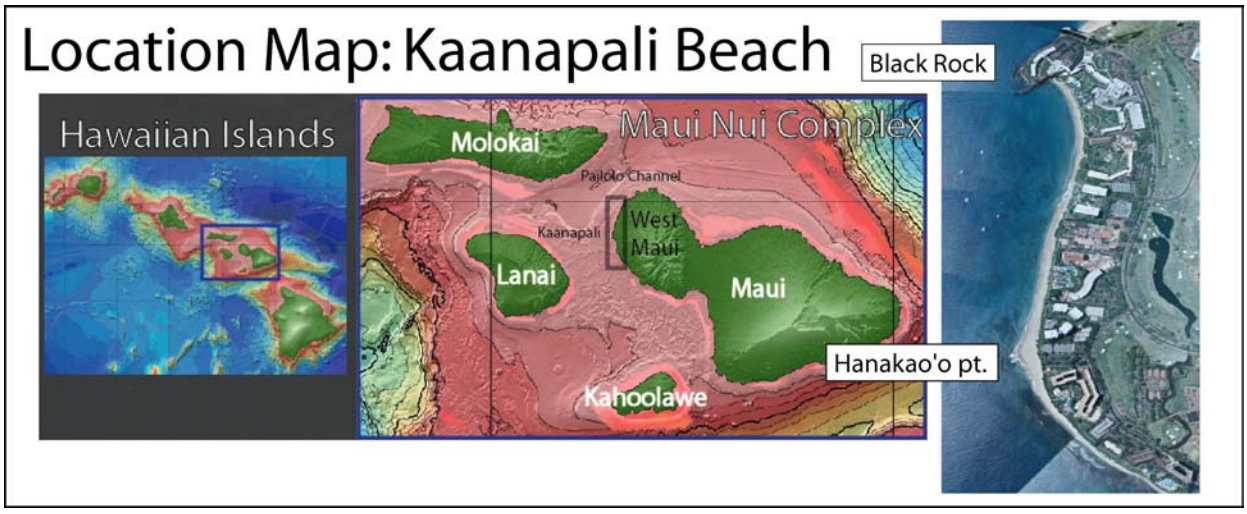

Figure 1 –Hawaiian Islands, Maui Nui, and Kaanapali.

Like the wave field, the Maui Nui current field is also spatially complex due to mean flows through the Pailolo Channel, which have been investigated in (Flament et al. 1996; Sun 1996; Storlazzi et al. 2006). Eversole (2003) characterized Kaanapali as an alongshore system that transports approximately 30,000 m^3 of sand to the north during summer months driven by

south swell, which later returns to the south in winter months forced by north swell. This volume of sand can result in dramatic beach width changes of more than 50 m at Hanakao'o Point over the course of the year.

Erosion Event

In early July 2003, Kaanapali experienced a rapid-onset erosion event that undermined resort landscaping and infrastructure landward of Hanakao'o Point (**Figure 2**).

Figure 2 - Erosion event July 2003 at Hanakao'o Point.

This event was likely the result of unusually high sea levels resulting from a series of mesoscale eddies that arrived over spring and summer months as seasonal sea level increased due to water column warming. Firing & Merrifield (2004), investigating mesoscale eddies using tide stations and satellite altimetry (shown in **Figure 3**), found that mesoscale eddies can persist for weeks to months and produce sea levels 15-20 cm above normal.

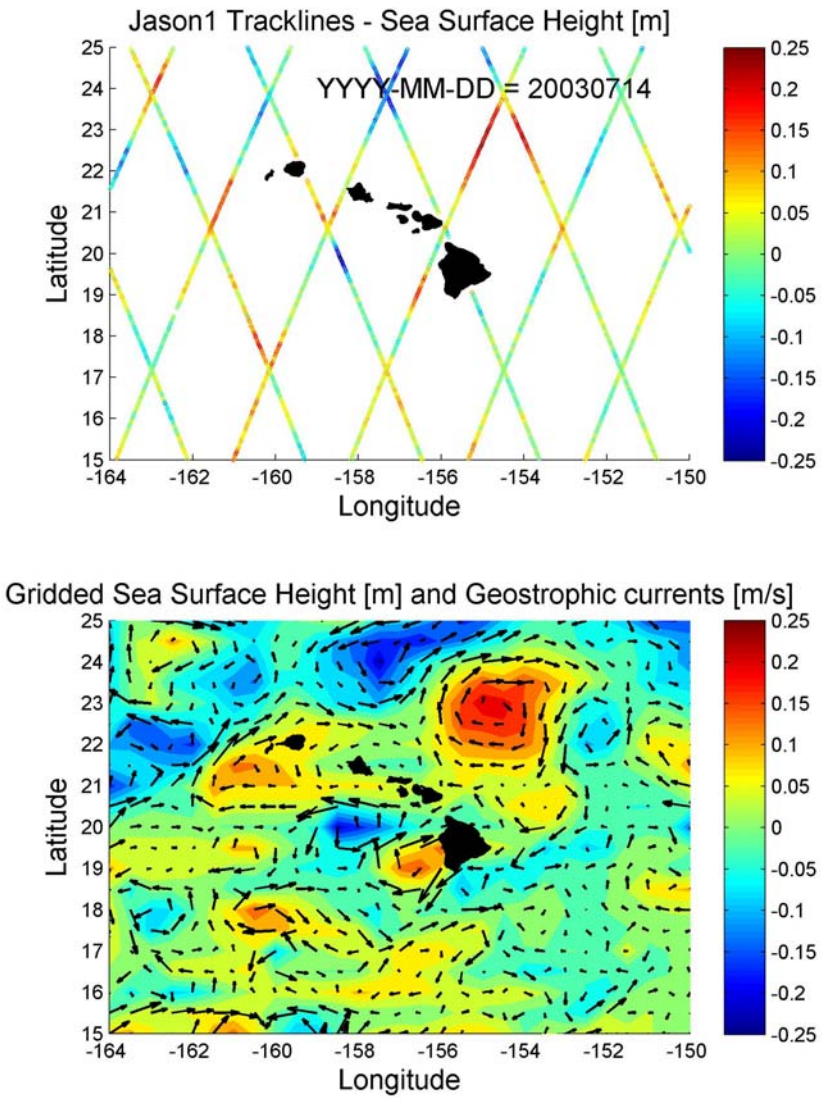

Figure 3 - Satellite altimetry map of sea surface height (SSH) in July 2003. Note the presence of the large eddy NW of the Hawaiian Islands.

The Kahului tide station on Maui reached its highest recorded hourly water levels during the mesoscale eddy sequence of 2003 (**Figure 4**).

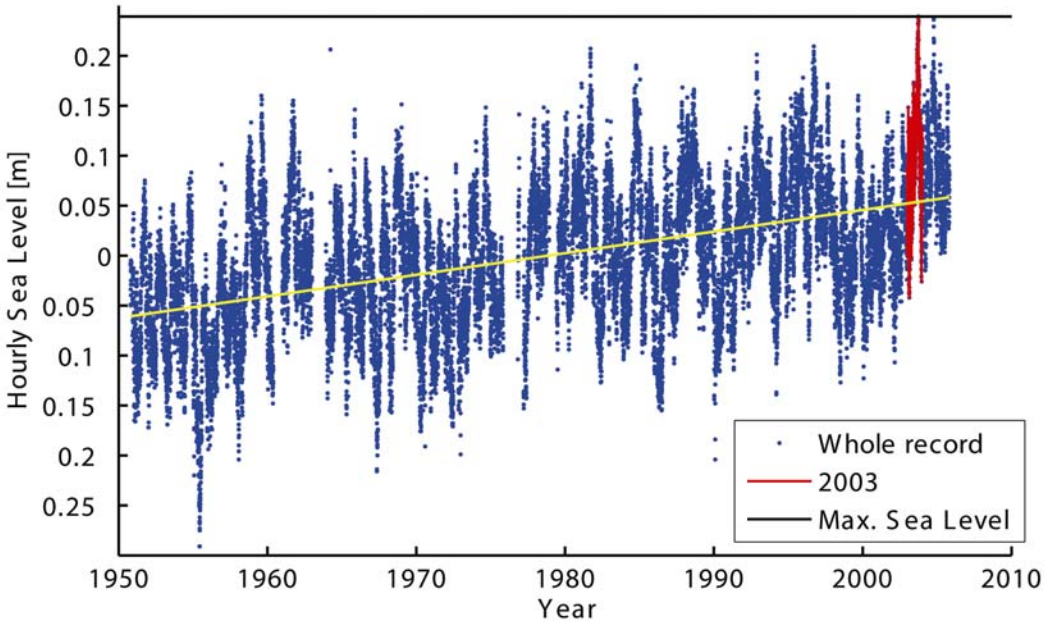

Figure 4 - Sea-level record from Kahului, Maui.

While 15-20 cm may seem like a small sea-level signal, in micro-tidal areas such as Hawaii (tide range = 0.6-0.8 m), these eddies represent a significant percentage of the tide range, and a significant increase on sandy shorelines otherwise exposed to nearly constant water levels. It is unlikely that the sea-level signal produced by these events would be able, by themselves, to cause significant erosion. However, when these coincide with spring tides and swell, the conditions for significant erosion exist. Mesoscale eddies are an episodic phenomenon today that represent a future permanent condition in coming decades due to eustatic sea-level rise on the order of 3 mm/year.

South swell during the July eddy in 2003 reached a significant wave height of only 0.75 m at 10 m water depth (Tp = 15 s, breaking wave height = 1.3 m), which is considerably lower than the annually recurring deep-water significant wave height of 2 m (Tp = 17 sec,

breaking wave height = 2 m). Wave heights on record in 2003 did not exceed typical seasonal wave heights (**Figure 5**).

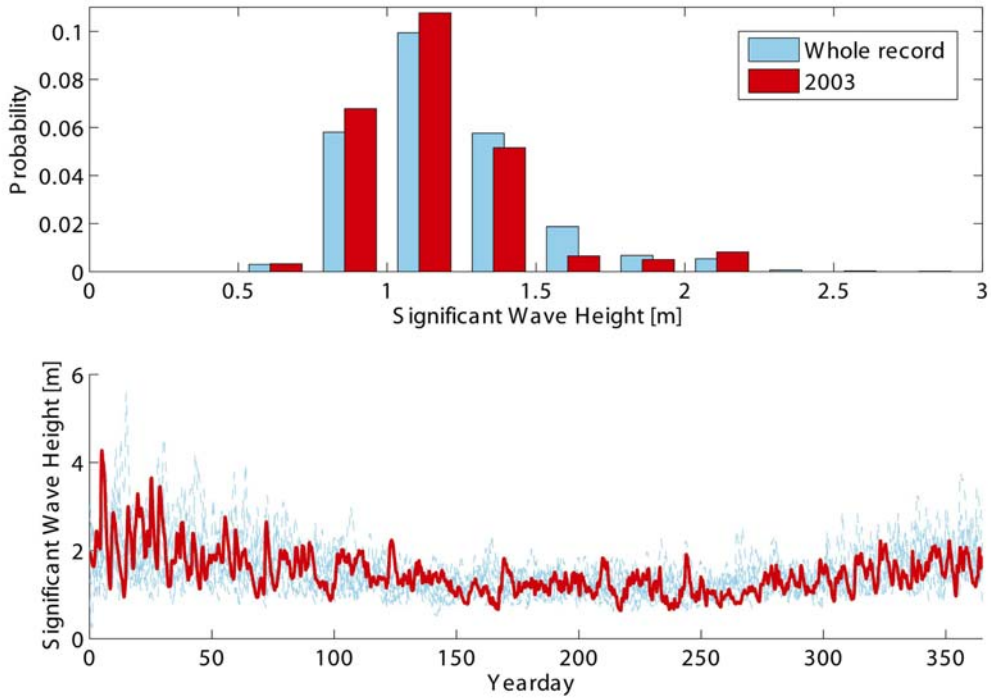

Figure 5 - Wave heights in 2003 (red) compared with typical seasonal cycle of wave heights (1990-2005)

These factors emphasize the importance of sea level as a contributing factor to erosion, and seem to be a clear case of unprecedented water levels in combination with uneventful waves leading to unprecedented erosion.

Seasonal Change

Seasonal profile changes at Kaanapali beach are pronounced. In winter months, north swell drives sand transport to the south where it accumulates a Hanakao'o point. In summer months south swell drives sand transport to the north where it accumulates at Black Rock. The seasonal changes in profile can be seen in aerial photographs (**Figure 6**).

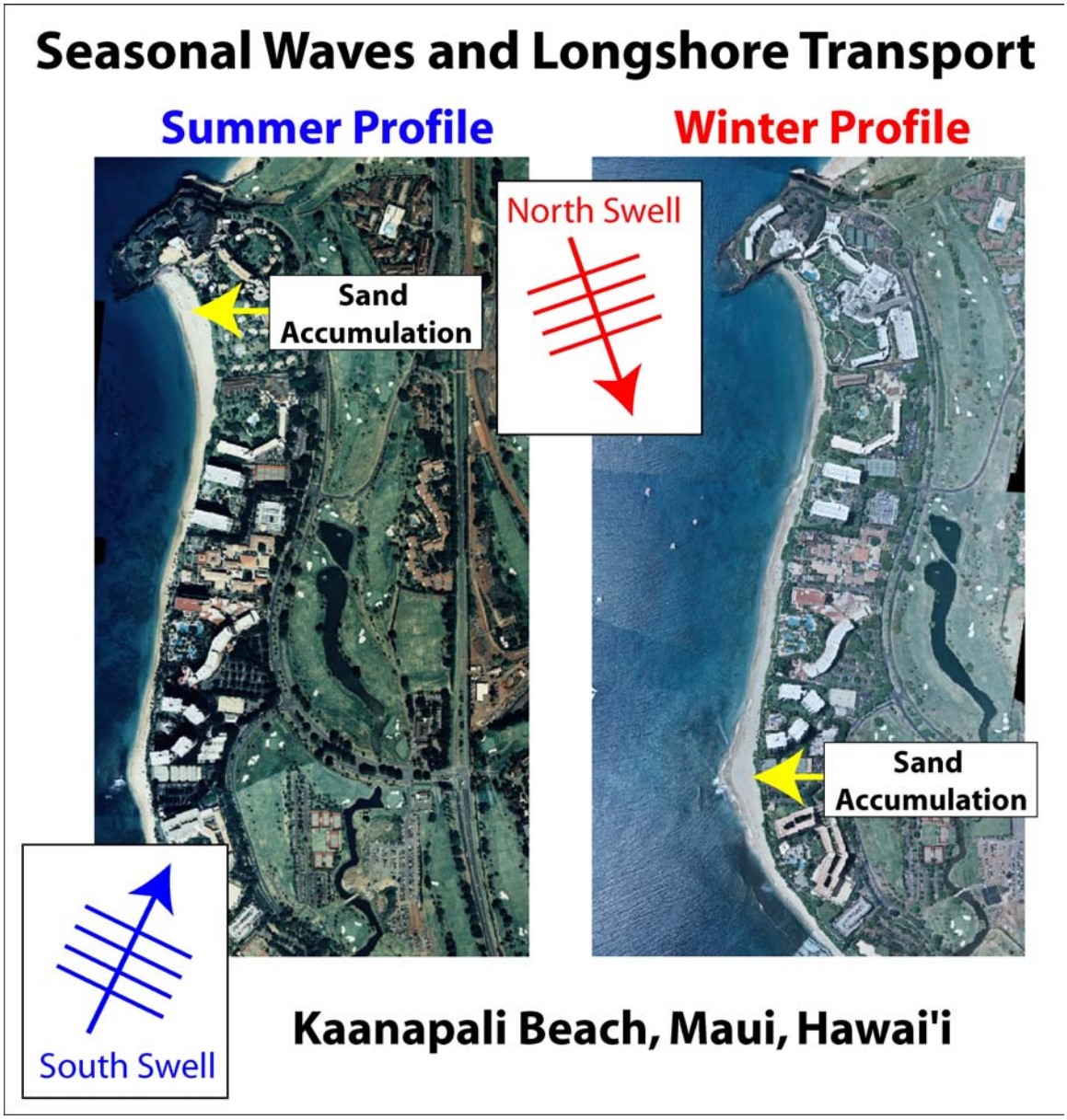

Figure 6 - Seasonal beach profile changes at Kaanapali Beach.

The accretion regimes can be idealized as two simple, different systems: accretion updrift of a headland (acting as a barrier to longshore transport, similar to a groin) and accretion on a flat fossil reef. Accretion updrift of a groin has been widely studied and is a common occurrence on coastlines in the US and abroad (U.S. Army Corps of Engineers 2002). The case of sand accretion on a perched beach is much less common, receiving only limited scientific attention (Eversole & Fletcher 2003).

Beach widening at Hanakao'o Point during winter months is an acute example of accretion on a perched beach, and poses one of the most interesting questions presented by the dynamic cycle of accretion and erosion at Kaanapali. Accretion at Hanakao'o is much more concentrated and dramatic than at Black Rock, even though the north end has an obvious accretion mechanism in place: the physical barrier of Black Rock. It is likely that the shallow, rough reef at Hanakao'o slows southward propagating alongshore currents generated by north swell leading to bed deposition. Hanakao'o also marks the point where swell regimes change from surging breakers in the northern portion of the beach at Black Rock where swash transport may play an important role in beach morphology to offshore dissipative breakers on the reef (characterizing the southern portion of the beach). Because of the difference in offshore depth and wave breaking characteristics, Hanakao'o likely marks the termination of swash zone transport. Improving an understanding of the various processes governing beach dynamics is critical to defining the role of eddy-generated water-level changes in episodic erosion.

METHODS

Data

An array of instruments shown in, including Conductivity, Temperature Depth (CTD/OBS) instruments and Acoustic Doppler Current Profilers (ADCP), was deployed at the 10 m depth contour along West Maui in 2003 as part of the USGS coral reef project to monitor physical processes affecting formation and lifespan of coral reef systems (Storlazzi et al., 2006). Another ADCP was deployed at Kaanapali in the summer of 2006 for further monitoring of waves and currents in shallow water.

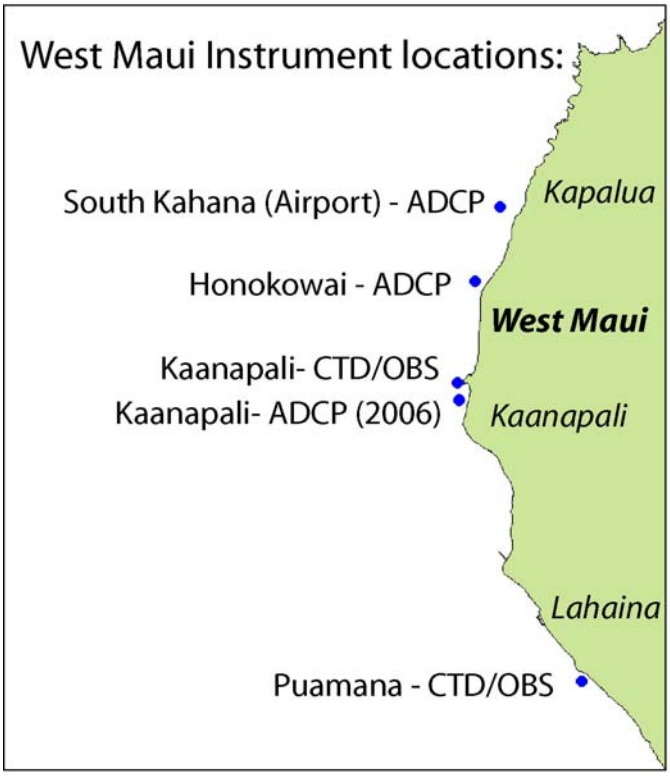

Figure 7 - West Maui instrument deployments in 2003.

For morphologic calibration we use beach profiles at Kaanapali from Eversole and Fletcher 2003. Monthly beach profiles were conducted from March 2000 to April 2001. The profiles were measured with a Geodimiter® total station and a 7 m telescoping rod. Shore normal transects were spaced every 2 m or at specific shoreline features including changes in slope on the subaerial beach and extended to a water depth of 5 to 7 m.

Modeling

The Delft3D-FLOW module (v. 3.24.03 used here) solves the unsteady shallow-water equations with the hydrostatic and Boussinesq assumptions. In 2D mode the model solves two horizontal momentum equations (see Eq. 1-2), a continuity equation (Eq. 3) and a transport (advection-diffusion) equation (Eq. 4) shown below:

$$\frac{\partial u}{\partial t}+u\frac{\partial u}{\partial x}+v\frac{\partial u}{\partial y}+g\frac{\partial \eta}{\partial x}-fv+\frac{\tau_{bx}}{\rho_w(h+\eta)}-\frac{F_x}{\rho_w(h+\eta)}-\nu_e(\frac{\partial^2 u}{\partial x^2}+\frac{\partial^2 u}{\partial y^2})=0 \quad (1)$$

$$\frac{\partial v}{\partial t}+u\frac{\partial v}{\partial x}+v\frac{\partial v}{\partial y}+g\frac{\partial \eta}{\partial y}-fu+\frac{\tau_{by}}{\rho_w(h+\eta)}-\frac{F_y}{\rho_w(h+\eta)}-\nu_e(\frac{\partial^2 v}{\partial x^2}+\frac{\partial^2 v}{\partial y^2})=0 \quad (2)$$

$$\frac{\partial \eta}{\partial t}+u\frac{\partial[(h+\eta)u]}{\partial x}+v\frac{\partial[(h+\eta)v]}{\partial y}=0 \quad (3)$$

$$\frac{\partial[hc]}{\partial t}+\frac{\partial[huc]}{\partial x}+\frac{\partial[hvc]}{\partial y}=h\left[\frac{\partial}{\partial x}\left(D_H\frac{\partial c}{\partial x}\right)+\frac{\partial}{\partial y}\left(D_H\frac{\partial c}{\partial y}\right)\right] \quad (4)$$

where u and v = the horizontal velocities in the x and y directions respectively; t = time; g = gravity; η = free surface height; h = water depth; f = coriolis force; ρ_w = density of water; τ_b = bed friction; F = external forces due to wind and waves, ν_e = horizontal eddy viscosity; D_H = horizontal eddy diffusivity; and c = concentration of suspended sediment. The equations are solved on a staggered finite difference grid using the Alternating Direction Implicit (ADI) method after Stelling (1984).

Computational Grids

The computations of Delft3D are performed on orthogonal curvilinear grids shown in. Modeling for this project involves two flow grids: a regional model covering the West Maui coast (**Figure 8**) and a local Kaanapali model (**Figure 9**). These grids are linked either by domain decomposition (DD) or interpolation of boundary conditions from the regional grid to the local grid. The use of DD models is very elegant, although primarily used here to validate the flow field in the smaller models, and justify the use of the local grid by itself. The use of just a local grid for simulations offers an improvement in computation time over

domain decomposition models, especially if the single domain models return results similar to the DD models.

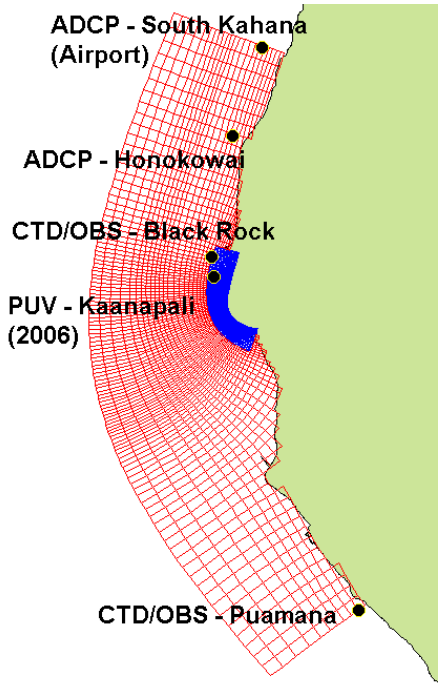

Figure 8 - Instrument locations and grid layout for West Maui model.

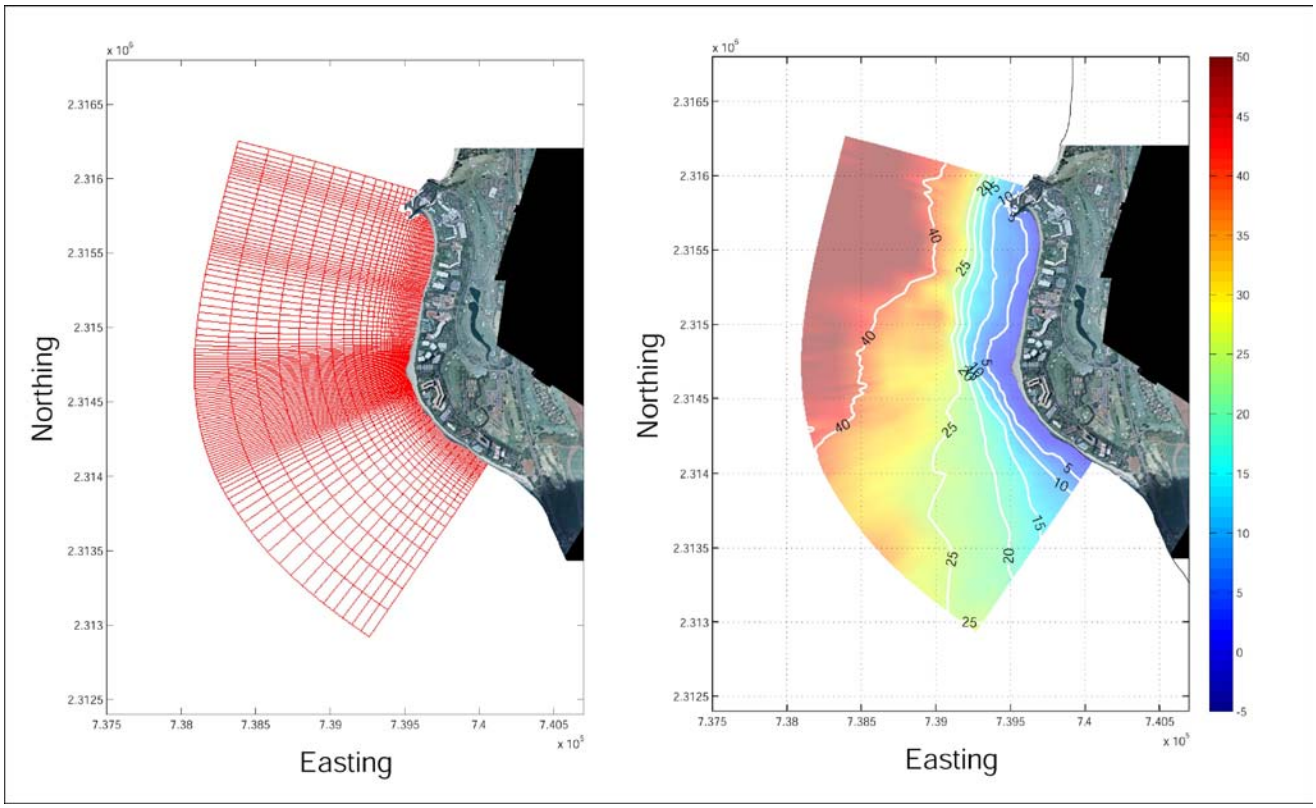

Figure 9 - Nearshore grid and bathymetry for model of Kaanapali

Table 1 - Model Parameters

Model Parameters			
Grid parameters		**Sediment properties**	
Resolution (West Maui Grid)	[300 m offshore 50 m nearshore]	median diameter D50 - [mm]	0.23
Resolution (Nearshore Kaanapali)	[150 m offshore 10 m nearshore]	sediment density [kg/m3]	2500
Flow parameters		**Morphology parameters**	
timestep [sec]	6	MorFac (Morphological Factor)	1
mode	2D	Dry cell erosion factor	1
gravity [m/s2]	9.81	Transport Formulations	Van Rijn 1993
water density [kg/m3]	1025	Current related bed load	1
bed roughness [Chezy - m1/2/s]	[(50-65)-sand (25-30)-reef]	Current related suspended load	1
horizontal eddy viscosity [m2/s]	0.1 - 1	Wave related bed load	0
horizontal eddy diffusivity [m2/s]	0.1 - 1	Wave related suspended loads	0
Threshold depth [m]	0.1-0.2		

Boundary Conditions

West Maui experiences a propagating tide, where gradient phases and amplitudes of tidal constituents exist along the coast, and tidal velocities are directed shore parallel (Storlazzi et al., 2006). Boundary conditions ideal for modeling this particular tidal configuration have been expressed in Roelvink and Walstra (2004), using water-level boundaries at the open (offshore) boundary and water-level gradient (Neumann) boundary conditions at lateral boundaries to solve for alongshore tidal velocities (**Figure 10**).

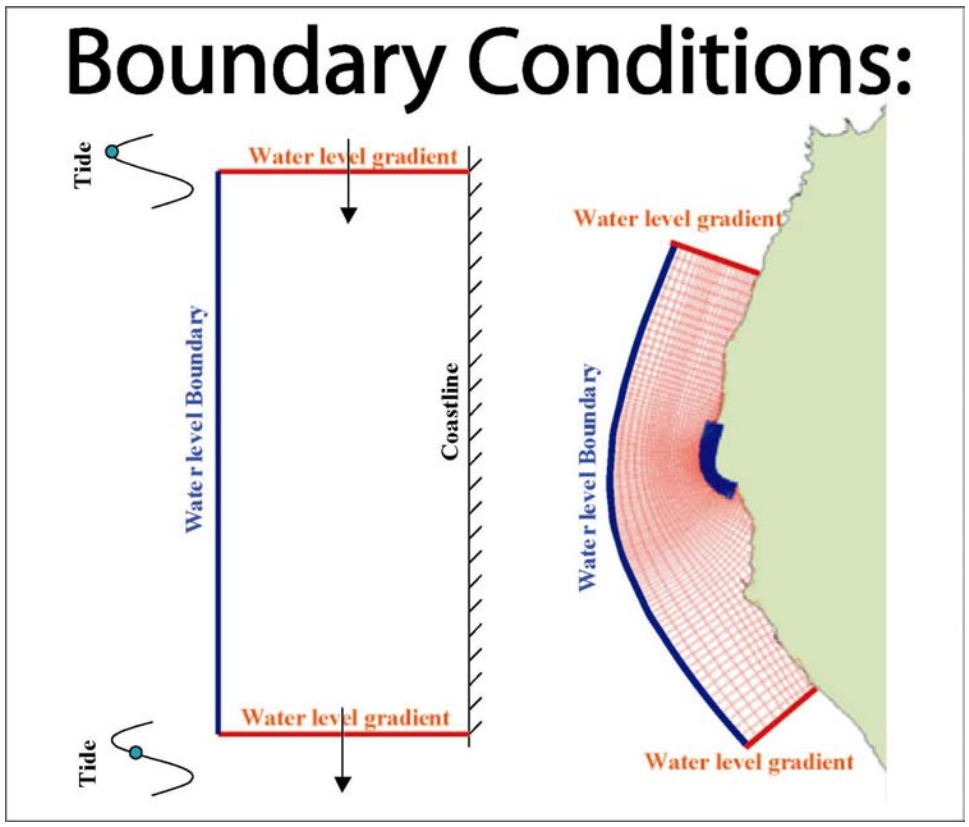

Figure 10 - Setup of boundary conditions

The boundaries use a harmonic forcing type, which facilitates use of the harmonic tidal components in water-level boundaries and determining water-level gradients. Water-level gradient boundary conditions can be determined simply from the amplitudes and phases

of the tidal constitutes at each lateral boundary using the equations given in Roelvink and Walstra (2004):

	Given tidal constituent	Gradient amplitude:	
Amplitude:	η_i	$\eta_i \left(\frac{\phi_i^{north} - \phi_i^{south}}{d_{ts}} \right)$	(5)
Phase:	ϕ_i	$\phi_i + \pi / 2$	(6)

where η_i = amplitude of the tidal constituent (m); ϕ_i = phase of the tidal constituent ($\phi_i^{north}, \phi_i^{south}$ for north and south boundaries respectively (radians)) and d_{ts} = distance between the lateral boundaries (m). With these boundary conditions prescribed, the bed roughness is tuned to match the observed current magnitude. These boundary conditions have been shown to provide accurate simulations of tidal velocities in Roelvink and Walstra's modeling studies (2004) at Egmond (Netherlands). This study provides another example of the excellent performance of boundary conditions developed from this scheme (see Results).

The wave boundary conditions are determined from model hindcasts (WaveWatch III) because there are no recorded buoy observations that include wave direction. These hindcasts adequately resolve observed wave heights and periods at a number of buoy locations in Hawaii. In this study, hindcast values of significant wave height, peak period and direction are applied uniformly at the open boundaries of the largest SWAN model, and a series of nested grids resolve the wave field down to the nearshore scale (10m grid) at West Maui and Kaanapali Beach. The SWAN nesting scheme is shown on **Figure 11**.

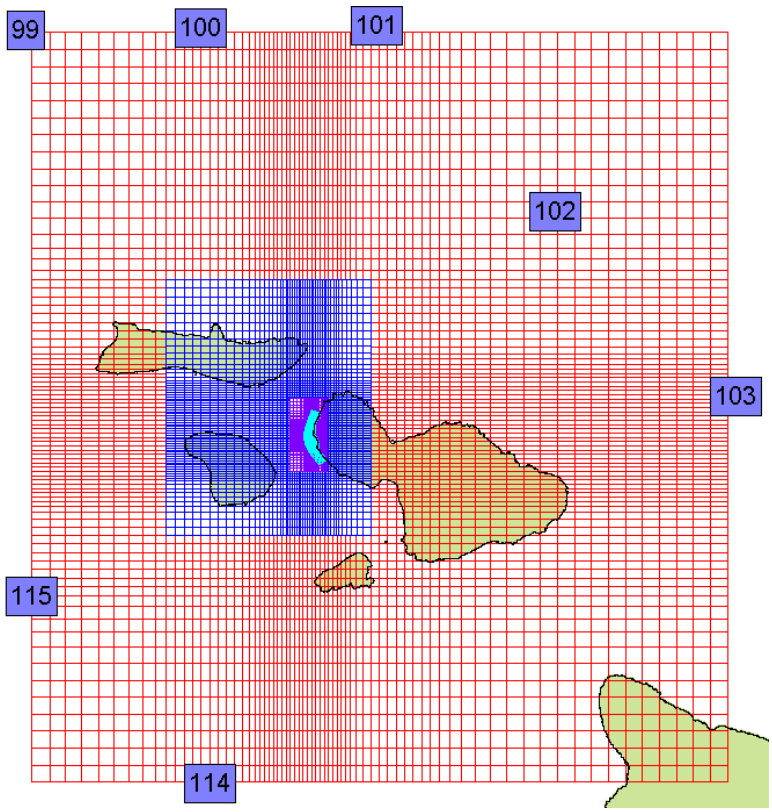

Figure 11 - SWAN nesting scheme. WaveWatch III hindcast locations are shown in boxes.

RESULTS

Model calibration has been carried out with the USGS data set. The model shows good comparison to the observed data set for tidal water levels, wave heights, and currents. Good comparisons of tidal water levels are readily achieved with the use of a water-level boundary at the open boundary. The modeled and observed tidal components at the instrument location are shown in **Table 2**.

Table 2 - Observed vs. modeled tidal constituents at instrument locations

Airport

	Obs Amp [m]	Mod Amp [m]	Obs Phase [deg]	Mod Phase [deg]
M2	0.175	0.173	-124.1	-124.0
N2	0.029	0.029	157.9	157.7
S2	0.062	0.061	79.4	79.4
K1	0.182	0.181	79.4	79.2
P1	0.048	0.048	85.9	85.1
O1	0.105	0.105	-148.2	-148.5
K2	0.029	0.028	-107.5	-108.3

Honokowai

	Obs Amp [m]	Mod Amp [m]	Obs Phase [deg]	Mod Phase [deg]
M2	0.176	0.174	-122.6	-121.6
N2	0.029	0.029	159.1	160.3
S2	0.061	0.06	81.2	82.1
K1	0.18	0.18	79.0	78.6
P1	0.048	0.048	86.3	85.3
O1	0.105	0.104	-148.5	-148.9
K2	0.028	0.028	-107.1	-106.6

Black Rock

	Obs Amp [m]	Mod Amp [m]	Obs Phase [deg]	Mod Phase [deg]
M2	0.177	0.174	-119.3	-118.3
N2	0.029	0.029	161.1	163.6
S2	0.059	0.058	85.3	86.0
K1	0.178	0.177	78.9	77.7
P1	0.048	0.047	86.9	85.2
O1	0.104	0.102	-148.3	-149.3
K2	0.027	0.027	-106.3	-103.7

Puamana

	Obs Amp [m]	Mod Amp [m]	Obs Phase [deg]	Mod Phase [deg]
M2	0.179	0.177	-107.4	-106.8
N2	0.028	0.029	174.4	175.8
S2	0.052	0.052	100.0	100.6
K1	0.168	0.169	75.0	74.9
P1	0.045	0.045	84.4	85.0
O1	0.096	0.096	-150.8	-150.9
K2	0.025	0.025	-95.4	-93.4

Agreement between modeled and observed currents is more difficult to achieve because of unresolved current-generating sources including mean flows through the Pailolo channel, internal tides, and the influence of the mesoscale eddy. Nevertheless the model shows good comparison with the observed currents, especially for Honokowai station, which is dominated by barotropic flow, shown in **Figure 12** and **Figure 13**.

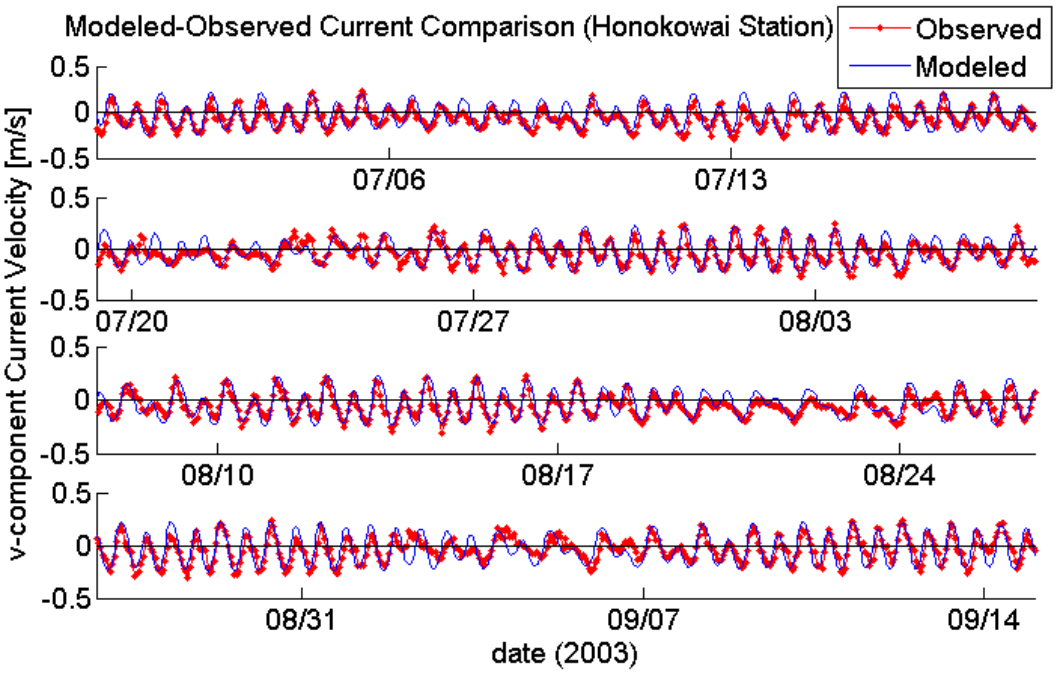

Figure 12 - Modeled vs. observed current comparison for Honokowai station.

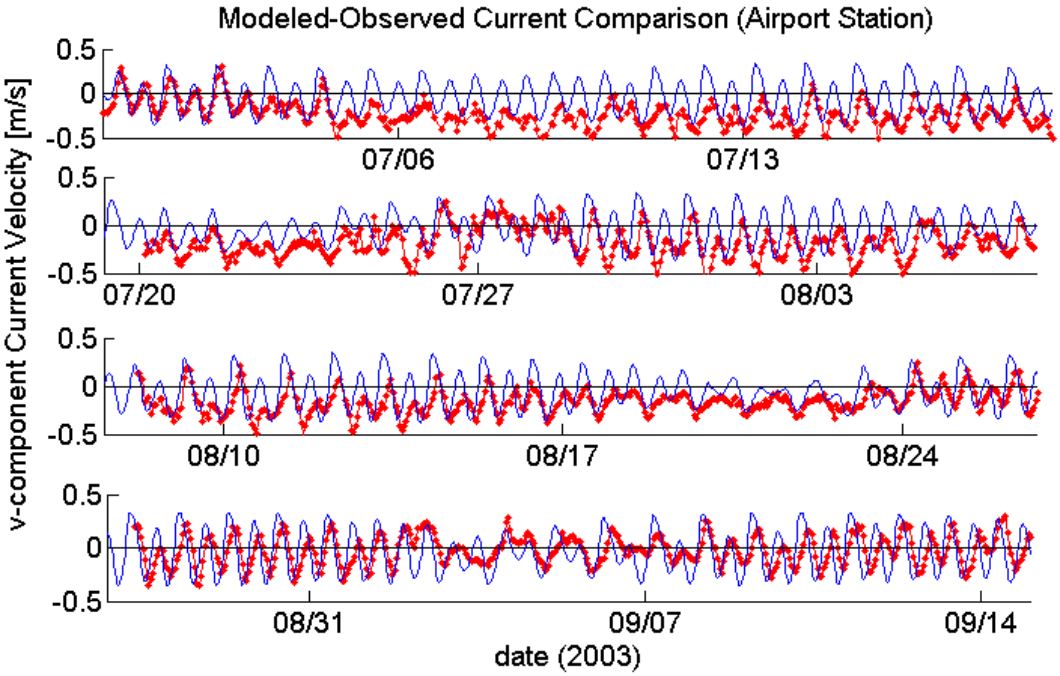

Figure 13 - Modeled vs. observed current comparison for the South Kahana (Airport) station.

Use of the SWAN model appears to resolve spatial variability around and inside of the Maui Nui complex. Modeled wave heights show good comparison with observations at instrument locations shown in **Figure 14**.

Wave fields and mean wave generated currents (from the mean over several tidal cycles) from two swell scenarios (Hs = 7m from the North and Hs = 1.5 m from the South) are shown in **Figure 15** & **Figure 16**, which show significant longshore currents at Kaanapali. Longshore transport patterns visually emerge when tracking the movement of a flagged sediment fraction (**Figure 17**). Although elegant, this technique is more computationally expensive, as the advection scheme must be computed for two sediment fractions instead of just one.

Morphologic simulations under dominant north and south swell conditions are shown in **Figure 18** with aerial photographs of the seasonal beach states when these swell regimes dominate.

The computed longshore transport for a real-time simulation in 2003 is shown in **Figure 17**. The computed model profile evolution for a real-time simulation from March to June in 2001 vs. the observed profile evolution of the same time period is shown in **Figure 20**.

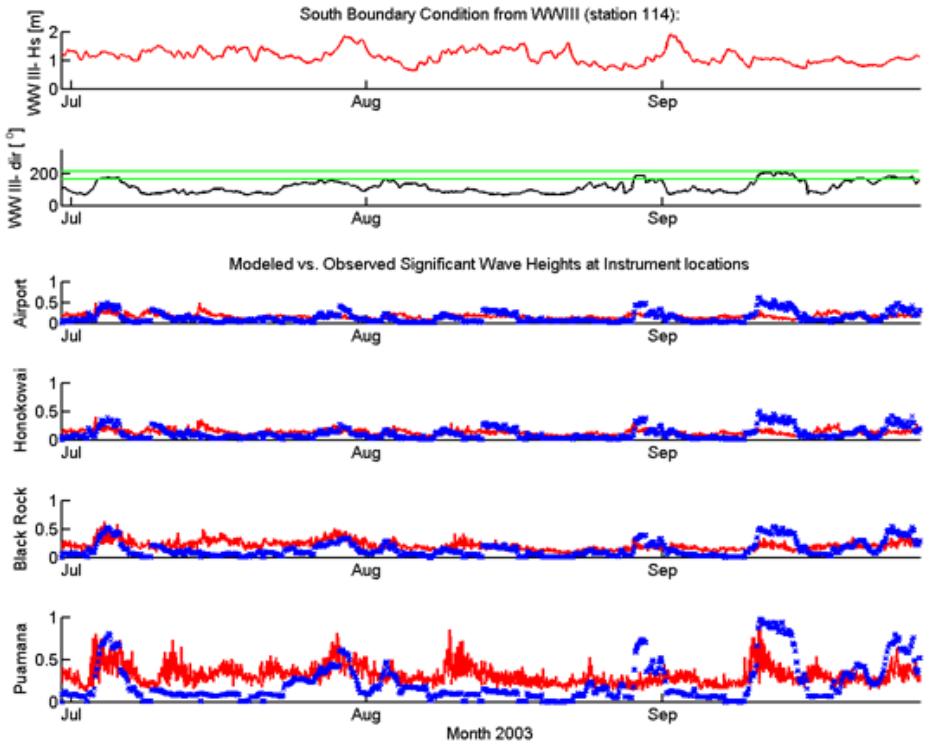

Figure 14 - WaveWatch III boundary conditions and comparisons of modeled (x) and observed (-) wave heights [m] at instrument locations. The lines on the second subplot represent the south swell window (170-210^{o}).

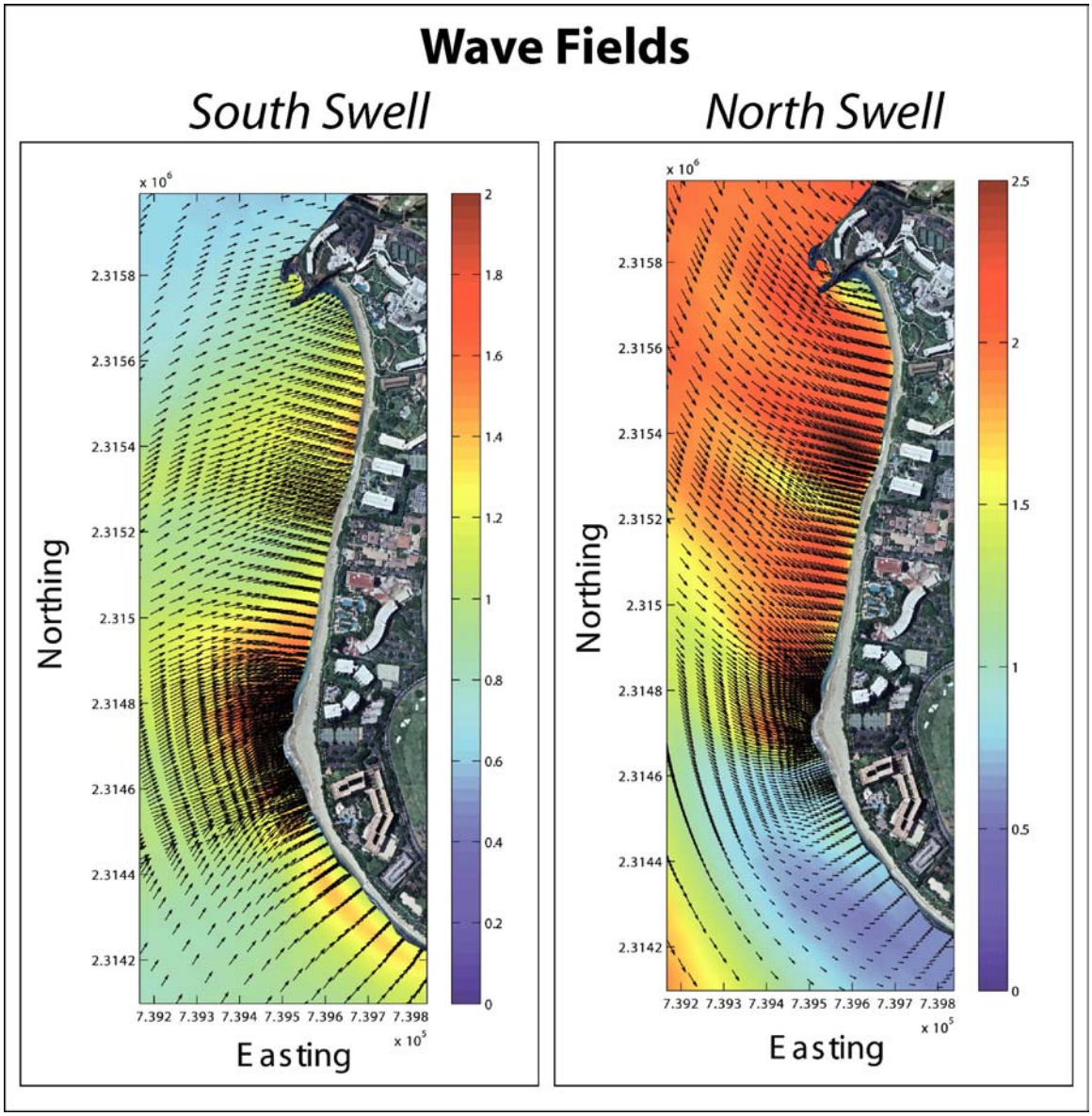

Figure 15 – Wave fields (wave height in [m]) at Kaanapali based on a South swell (Hs = 1.5 m) and a north swell (Hs = 7). Significant island blockage reduces the wave height at Kaanapali due to the north swell.

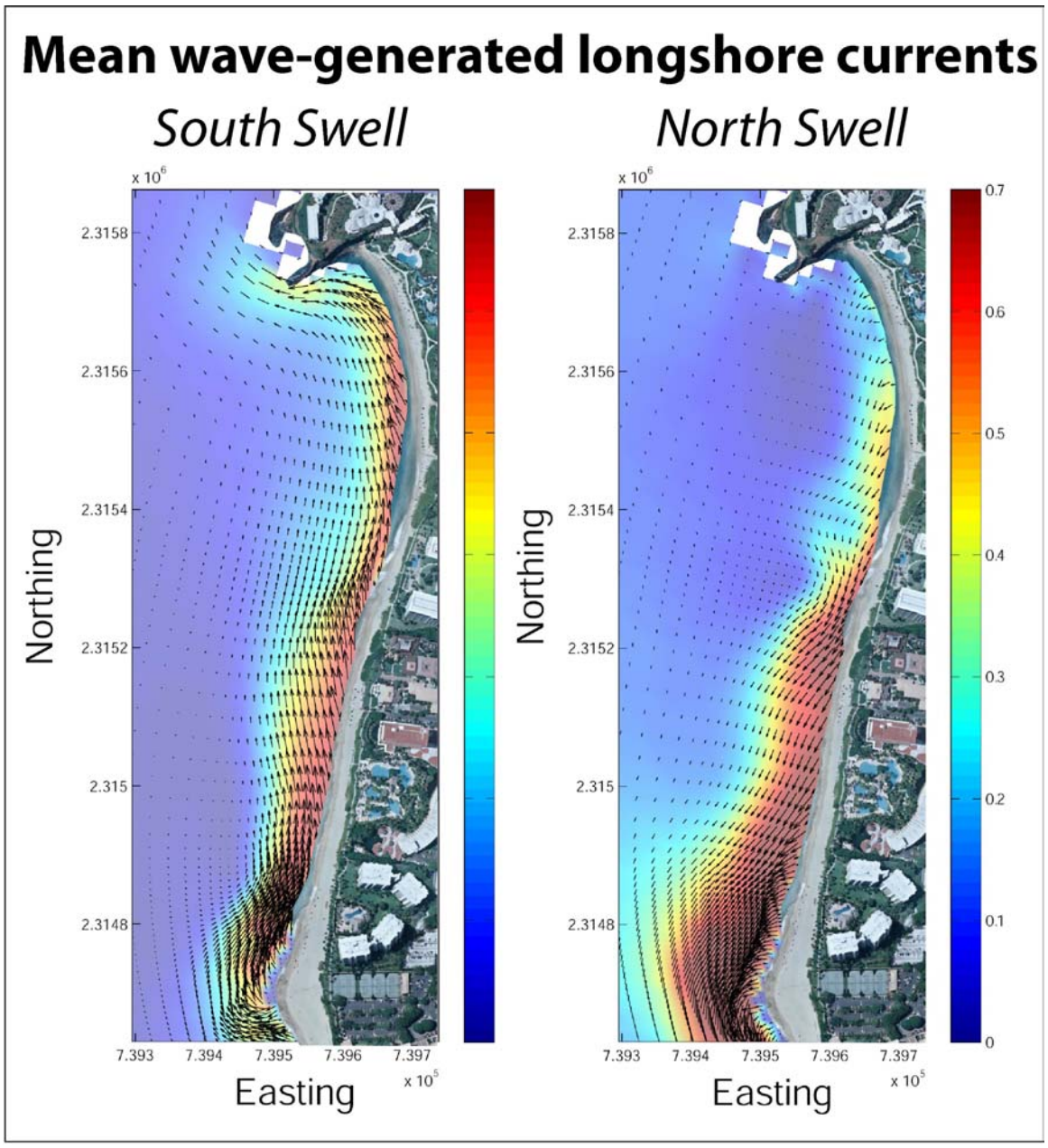

Figure 16 – Mean wave generated currents [m/s] for South and North swell at Kaanapali Beach

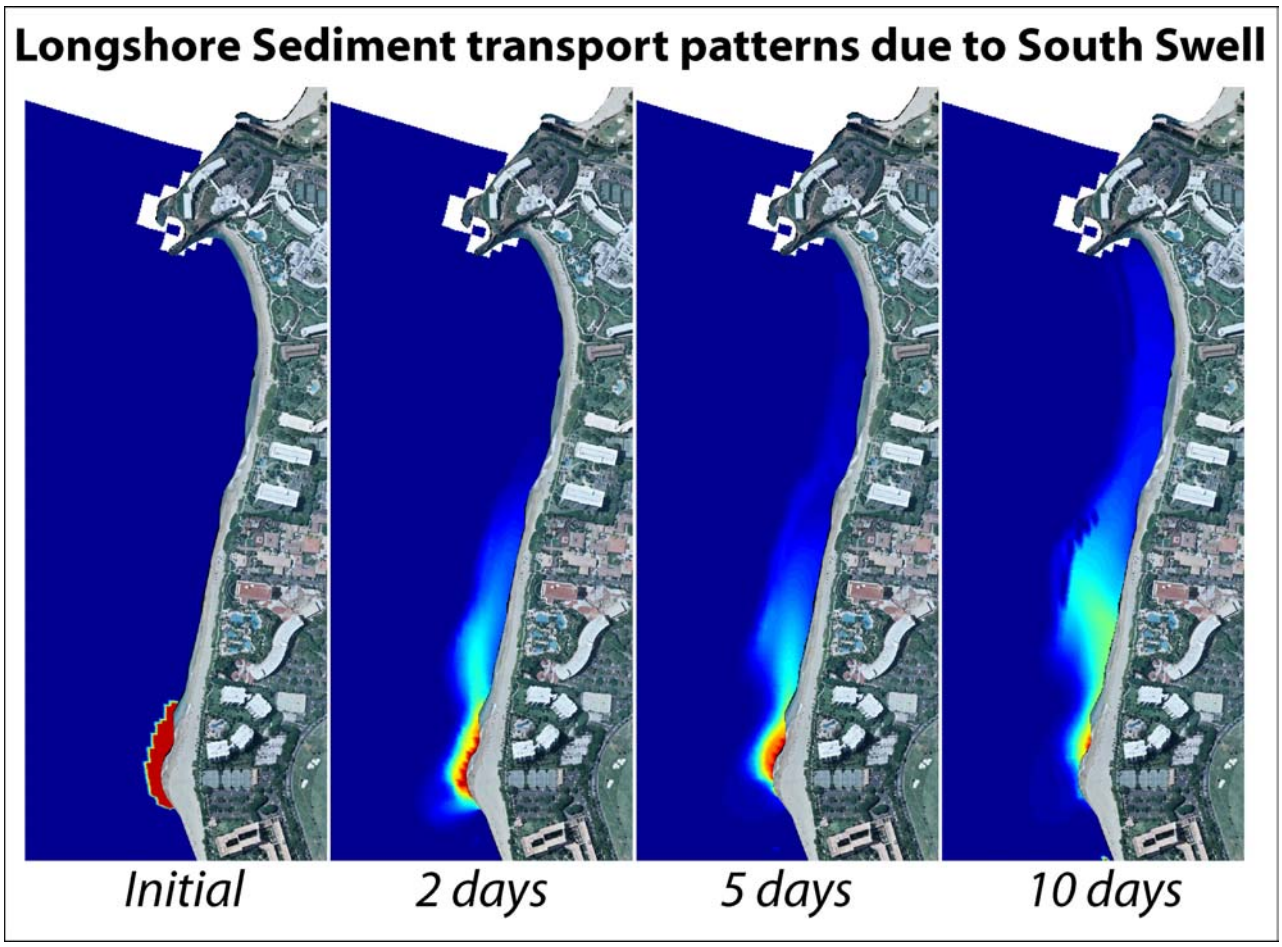

Figure 17 - Longshore Sediment transport patterns at Kaanapali. Tracked using a flagged patch of sand (in red - initial). Colormap represents fraction of flagged vs. unflagged sediment.

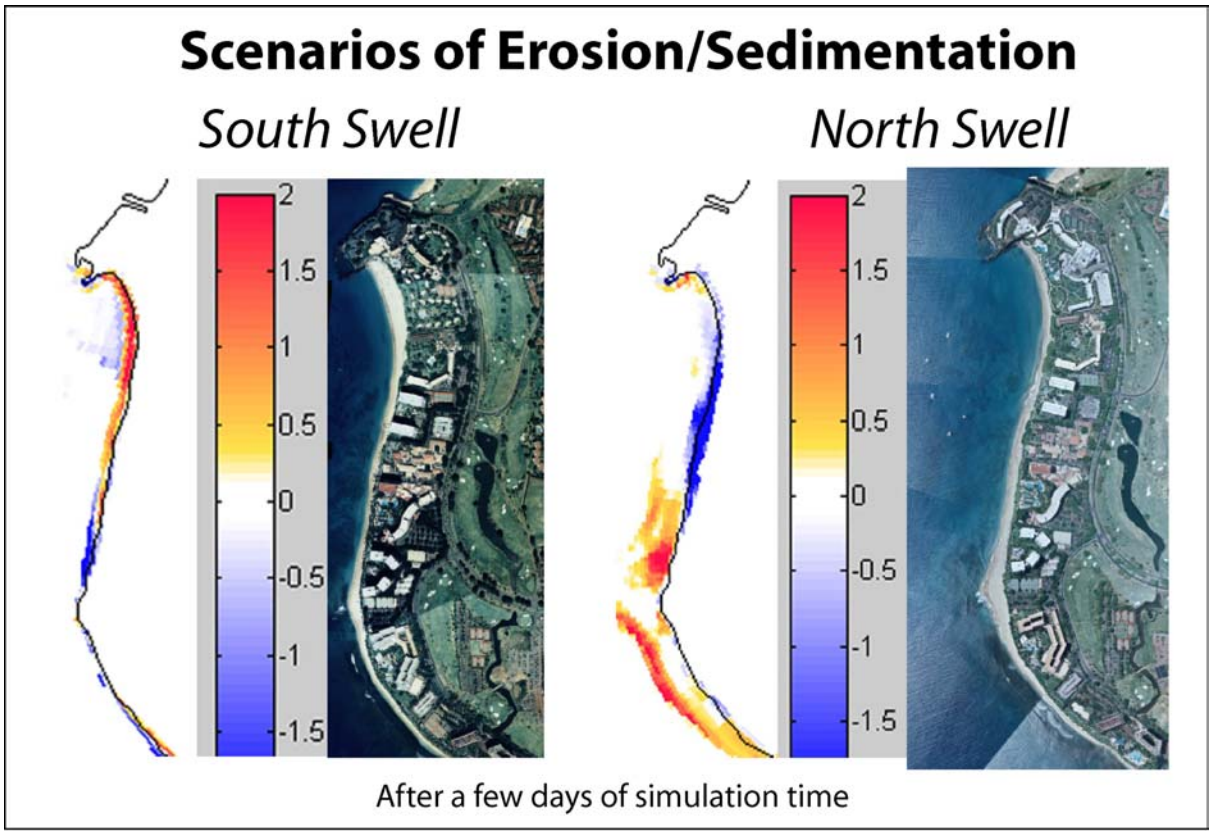

Figure 18 – Observed and simulated beach states during summer (left) and winter (right) swell conditions.

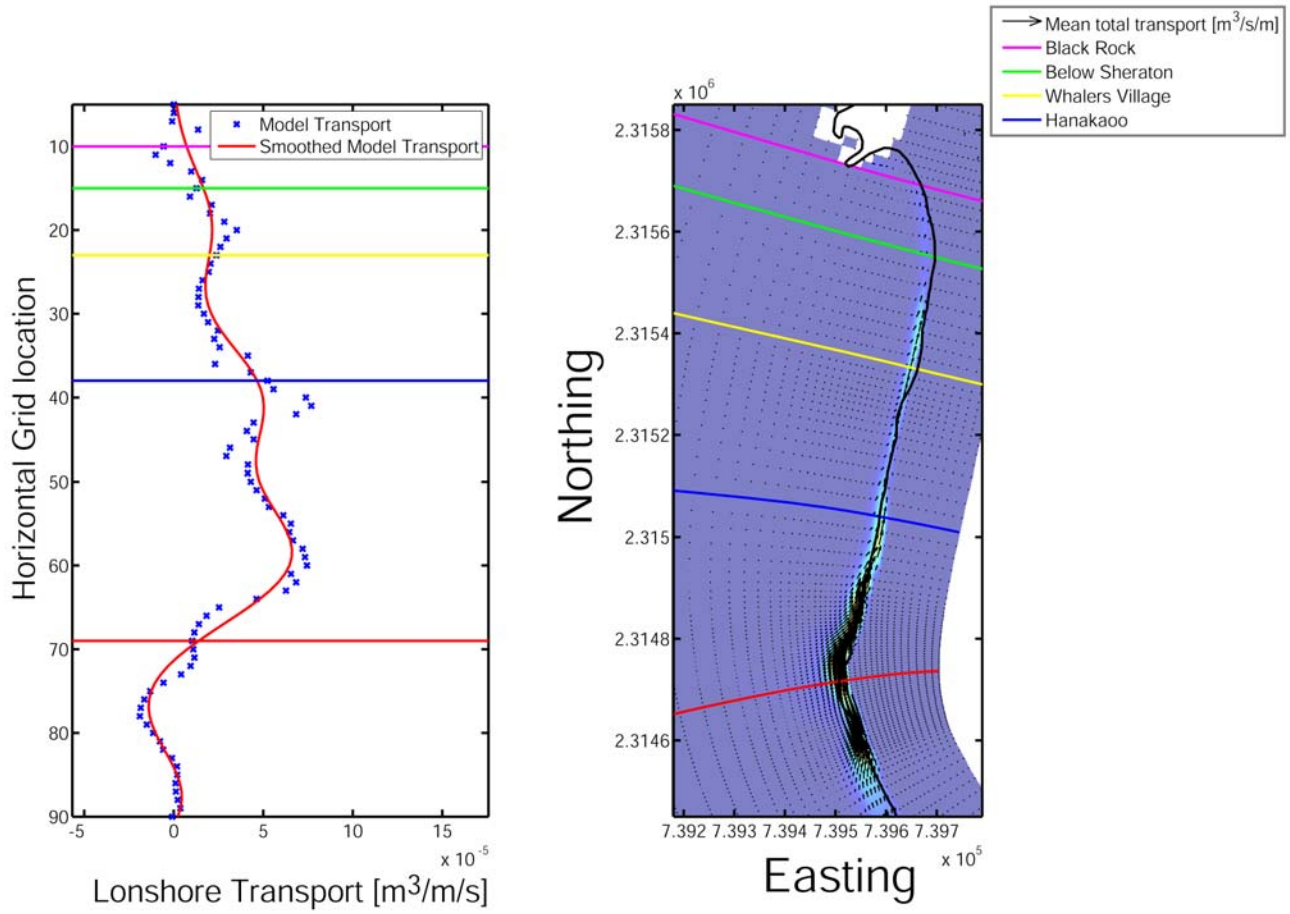

Figure 19 - Modeled longshore transport at Kaanapali for a real-time simulation summer 2003 (the year of the mesoscale eddy event).

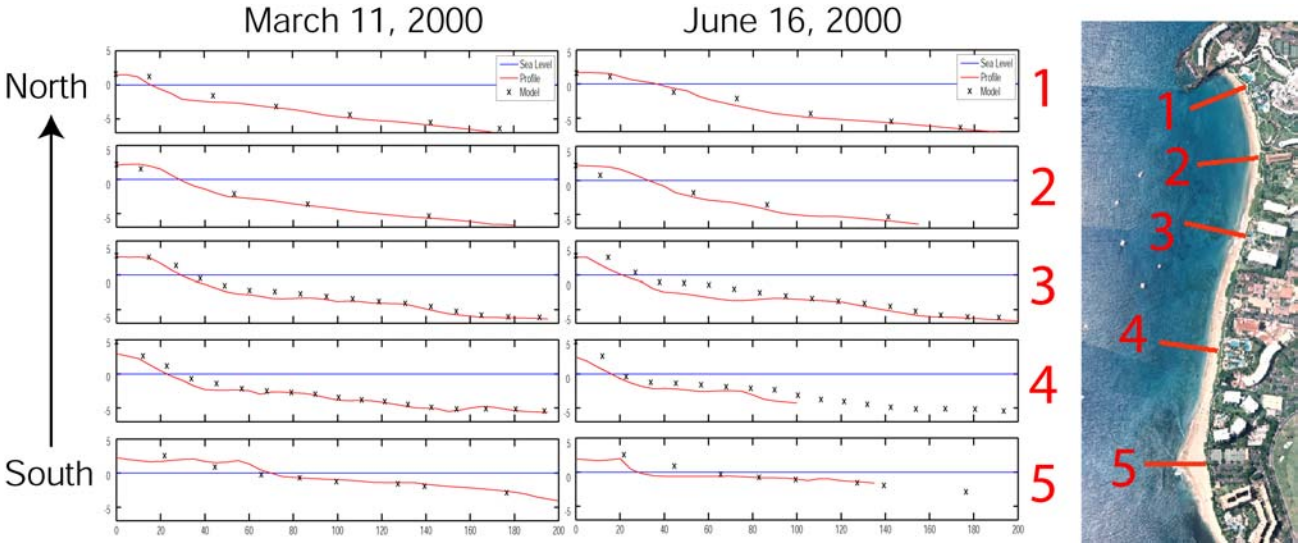

Figure 20 - Computed (x) vs. observed (red) beach profile evolution for the summer of 2000.

DISCUSSION

Using Delft3D with water-level gradient boundary conditions prescribed in Roelvink and Walstra (2004) provide excellent resolution of current velocities in regions dominated by barotropic tidal flow. For regions influenced by mean flows and internal tides, more physical processes need to be accounted for to better resolve observed velocities. It appears the Honokowai station (**Figure 12**) is well resolved, while the South Kahana (Airport) station (**Figure 13**) is influenced by the presence of mean flows and internal tides. Despite the influence of unresolved processes, the models show good comparison with the observed flow velocities.

Mean flows (derived from the observed time series with the harmonic components removed) observed at the South Kahana (Airport) Station appear to be related to wind direction, and may be related to island-trapped wave events (Merrifield 2002; Storlazzi 2006). **Figure 21** shows the time series of wind speed and mean flow and their inter-relationship.

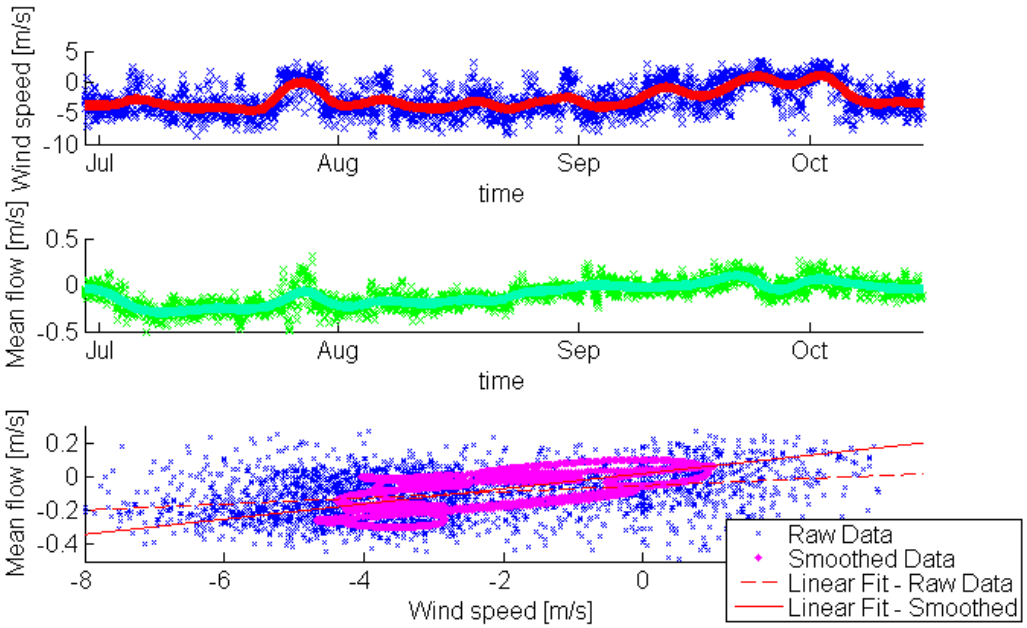

Figure 21 - Relationship between the vertical components of the winds and mean flow through the Pailolo Channel recorded in the South Kahana (Airport) station.

Wind speed and mean flow seem to mirror each other. A notable event in the time series is the decrease in wind speed in late July, which leads to a corresponding decrease in the mean flow through the channel. Although the model accounts for wind forcing, the mean flow is not resolved. If the mean flow is due to wind forcing, the inability to resolve the mean flow is probably due to the limited coverage of the model domain: inability to develop significant wind-generated currents, and/or the topographic influence of West Maui which may cause local acceleration of the wind field.

The mean flow observed at South Kahana seems unlikely, from the two observed time series, to extend past the Honokowai station and potentially affect currents and sand transport at Kaanapali Beach. The major influence in sand transport at Kaanapali seems to be the wave-generated currents that arise from obliquely incident waves from north and south swell breaking on the westward-facing shoreline.

The misfit between the observed and modeled wave heights along West Maui, shown in **Figure 14**, may result from using simulations from a larger model (WaveWatch III – referred to as WWIII) to force the smaller model. WWIII has been well-validated using buoy and altimetry data (Tolman 2002, Baird and Associates 2005, Tracy et. al. 2006). However, we do not have observation stations at the boundary locations of the small West Maui model to validate WWIII around this particular location. The two main discrepancies between modeled and observed wave height are that the model does not capture a few particular swell events, and a background wave height exists in the data that is not resolved in the model. The first issue may be cause by WWIII's inability to resolve swell direction adequately. Any slight deviation in swell direction and significant island blockage (shadowing) can significantly reduce the modeled wave heights around West Maui. The second issue may be due to the use of parametric wave conditions (a single significant wave height, period and direction) applied to the boundary. Currently Delft3D cannot use time-varying wave spectra as boundary conditions. Using parametric wave boundary conditions only resolves the dominant wave conditions, not the smaller background swell.

While simulations of shoreline accretion and erosion forced by the dominant swell regimes show a qualitative morphologic behavior, the ultimate goal of modeling is to reproduce or predict transport volumes and resulting changes in the beach profile. The default transport parameters of Delft3D predict a northward longshore transport of around 7,000 m^3 for the summer of 2000, which is around a factor of 4 lower than the observed transport of 30,000 m^3 for the summer of 2000 based on beach profiles of Eversole (2003). For calibration purposes, tuning model parameters to match the data, is often done, however unsatisfying the practice may be.

Modeling beach profile changes often captures observed changes in mean state, but is less successful at predicting significant erosion and accretion events (**Figure 20**). While the model seems to perform adequately for scenarios on timescales of a few days, variability of wave and current conditions on longer timescales make simulations on timescales of months to years more difficult to resolve. Long-term morphological modeling often use of techniques such as input reduction (reducing the tide & wave climate into a few dominant scenarios) to eliminate unimportant swell regimes and reduce computational time (Roelvink 2006). Comparisons of observed and modeled profile changes (in the vertical direction), in **Figure 22**, show that the model tends to over predict accretion (indicated by the frequency of records in quadrant 2 and above the perfect fit line) and to miss large erosion and accretion events in the end members of the littoral cell (Black Rock and Hanakao'o). Bias towards accretion is likely due to the persistence of small wave states during the 3-month simulation, and inability to resolve swell events that lead to significant change. The effects of 2D vs. 3D modeling on accretion predictions should also be investigated.

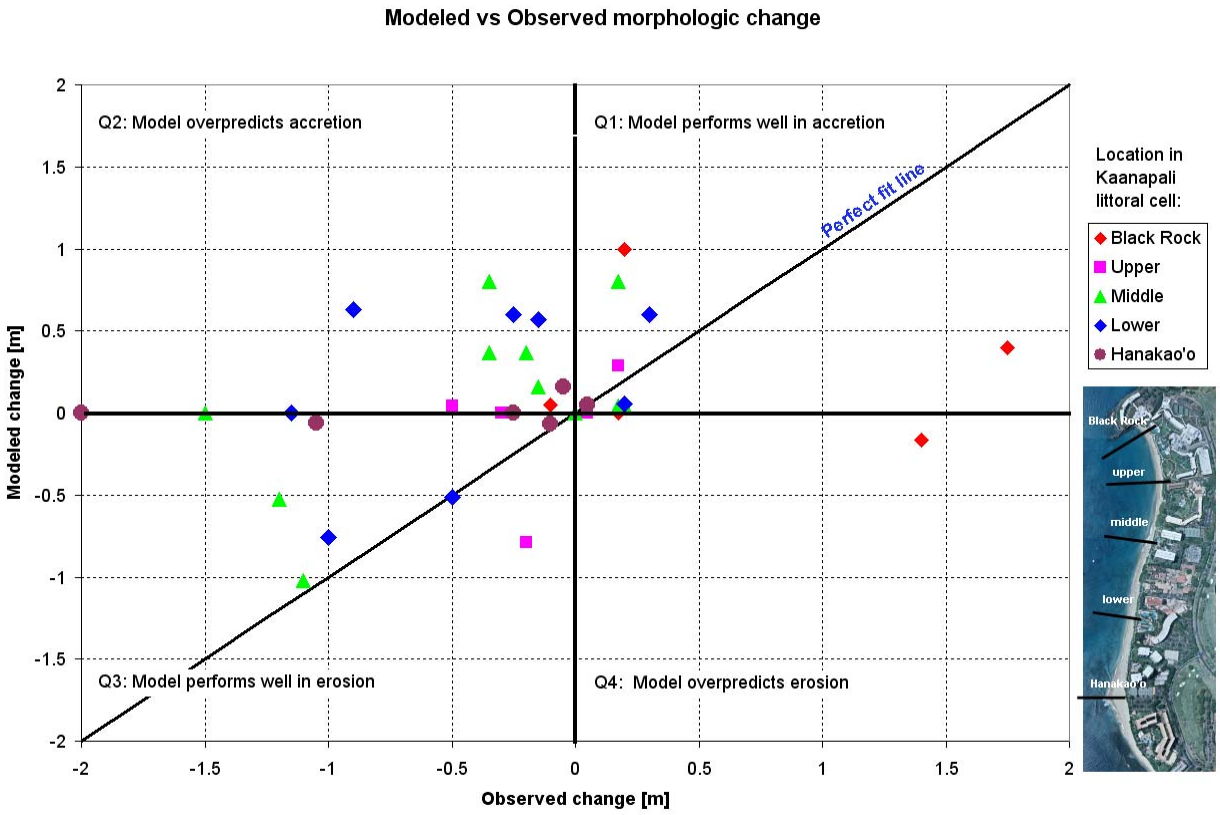

Figure 22 - Observed vs. modeled beach profile changes over 3 months at a number of locations at Kaanapali, Summer 2000.

Modeling the response to a small sea-level signal (such as one caused by the mesoscale eddy) yields no differences in computed transport and cumulative erosion sedimentation patterns due to this small signal. This is likely the result of discretization by the model. There is an inherent problem simulating natural processes using discrete numerical simulations, especially when variability of a particular process, in this case sea level in its vertical and horizontal position, exists on a smaller scale than the discrete grid is capable of resolving (**Figure 23**). A simple means of computing the grid cell resolution required to flood a previously dry grid cell due to a small sea-level rise can be thought of as the sea-level rise divided by the beach slope. For steep beach profiles (1/8) such as

Kaanapali, and small sea-level signals due to mesoscale eddies (~15 cm) a grid cell resolution of 1.2 m is required. Such fine grid cell resolutions are extremely computationally expensive, especially as they are subject to stability criteria, which require a proportionally small time discretization as spatial discretization. Our nearshore Kaanapali grid has resolution around 10 m, which is significantly coarser than the required resolution.

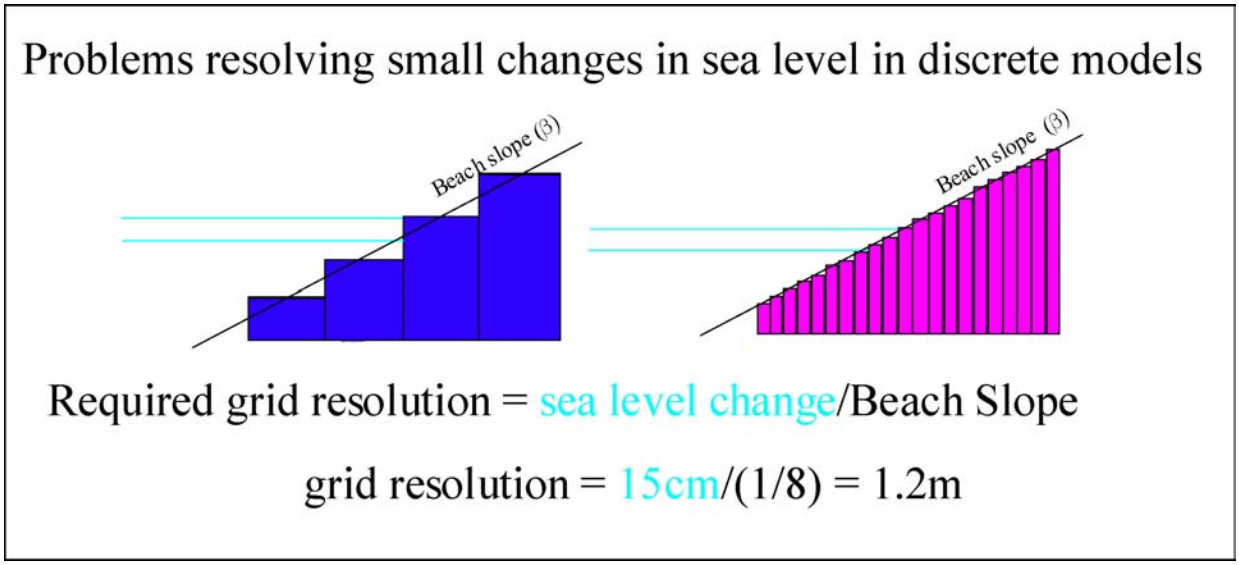

Figure 23 - Illustration of problems resolving small sea level changes in discrete grid based models.

Another process we are not effectively resolving in the model is the action of swash transport producing morphologic changes in the beach face. The model does, however, have a scheme to replicate morphologic beach face changes by applying a relative amount of erosion or accretion in wet grid cells to adjacent dry grid cells. While this scheme is a practical solution to an extremely complex problem, it does leave a potentially important processes unresolved.

We can, however, make interesting conclusions about sand transport from simulations of simple scenarios. Morphologic simulations of transport due to north swell with a uniform

bed roughness demonstrate transport of a considerable amount of sand around Hanakao'o Point. Increasing the simulated roughness for the submerged fossil reef offshore (making it spatially variable) from Hanakao'o Point causes the sand to accumulate in this location. This is consistent with field observations.

Inability of the model to resolve the signal of the mesoscale eddy should not cause us to dismiss its influence. Simple Bruunian models assign sea-level position paramount influence, although the presence of reef surfaces may change this simple dynamic. It appears that increased sea level on a normal shoreline profile (not perched) may exist in unstable equilibrium until wave energy initiates transfer to a new position. The duration of mesoscale eddies is sufficient to begin this transition as evidenced by the considerable erosion observed in summer 2003 at Kaanapali. The event also suggests that increased sea-level signals may cause accelerated seasonal response in alongshore systems.

CONCLUSIONS

Robust numerical models allow for realistic shoreline change simulations. Adequate observations are indispensable to ensure realistic performance. Poor modeling performance arises from inadequate tuning, unresolved processes, and spatial discretization of continuous natural processes. Use of water-level gradient boundary conditions given by observations of tidal components and the equations used in Roelvink and Walstra (2004) successfully model tidal velocities. Scenario-based modeling of seasonal shoreline change is qualitatively successful, whereas real-time, long-term simulations often to not capture significant changes in beach profile and shoreline position.

Mesoscale eddies and accretion perched beaches atop rough reef substrates play a potentially significant role in beach morphology of Hawaiian shorelines, and merit continued investigation.

FUTURE WORK

The work presented here may be helpful in preparing future experiments to study approaching mesoscale eddies. Satellite altimetry takes a snapshot of the sea surface height of the entire globe every 10 days. Using this data, eddies approaching the islands can be identified and assessed for risk. If the eddies estimated arrival coincides with the start of the seasonal wave cycle and before significant beach profile changes have occurred, several nearshore wave and current instruments should be placed in an array at the particular beach. To accompany the instrumentation T-LIDAR beach surveys should be conducted at intermediate temporal resolution when swell is not expected, and at high temporal resolution (before, during and after) when swell is expected. The temporal resolution of T-LIDAR beach surveys should also attempt to resolve the beach profile changes as a function of the tide. It is expected that at high tide the wave runup may reach further on the beach, and potentially impact dunes and cause scarps to form. If these small sea-level signatures can lead to increased erosion, much larger erosion events may occur with the coincidence of these eddies, spring tides and large swell, rather than with large swell alone.

ACKNOWLEDGMENTS

The author would like to thank Edwin Elias, Dolan Eversole, Chris Conger, Jeff List, Capt. Joe Reich, Lamber Hulsen, Dano Roelvink, Dirk-Jan Walstra, Everyone at Delft3D support: Johan Dijkzeul, Arjen Luijendijk, and Meo de Rover.

REFERENCES

Baird and Associates. 2005. Pacific Ocean Wave Information Study Validation of Wave Model: Results Against Satellite Altimeter Data. Prepared for U.S. Army Corps of Engineers Engineering Research and Development Center

Elias, W.P.L. (2000). "Hydrodynamic validation of Delft2/3D with field measurements at Edmond," Proc. 27th ICCE, Sydney, Australia.

Elias, W.P.L. (2006). "Morphodynamics of Texel Inlet," Ph. D. thesis. Delft University of Technology, The Netherlands.

Eversole, D., Fletcher, C.H., (2003). "Longshore Sediment Transport Rates on a Reef-Fronted Beach: Field Data and Empirical Models Kaanapali Beach, Hawaii," Journal of Coastal Research: Vol. 19, No. 3, pp. 649–663.

Firing, Y. L., and Merrifield, M. A., (2004). "Extreme sea level events at Hawaii: Influence of mesoscale eddies," Geophys. Res. Lett. 31, L24306

Flament, P., Lumpkin, C., (1996). "Observations of currents through the Pailolo Channel: Implications for nutrient transport," In: Wiltse, W. (Ed.), Algal Blooms: Progress Report on Scientific Research, West Maui Watershed Management Project, pp. 57 –64.

Klein, M.D., Elias, E.P.L., Stive, M.J.F., Walstra, D.J.R., (2001). "Modelling inner surf zone hydrodynamics at Egmond, The Netherlands," In: Hanson, H., Larson, M. (Eds.), Proc. 4th Int. Conf. on Coastal Dynamics '01. ASCE, Reston, pp. 500–509.

Lesser, G.R., (2000). "Computation of Three-dimensional Suspended Sediment Transport within the DELFT3D-FLOW Module," Master's thesis. Delft University of Technology, The Netherlands.

Lesser, G.R., Roelvink, J.A., van Kester, J.A.T.M., Stelling G.S., (2004). "Development and validation of a three-dimensional morphological model," Coastal Engineering. v. 51. pp. 883–915.

Luijendijk, A.P., (2001). "Validation, calibration and evaluation of Delft3D-FLOW model with ferry measurements," Master's thesis. Delft University of Technology, The Netherlands.

Merrifield, M.A., Yang, L., Luther, D.S., (2002). "Numerical simulations of a storm generated island-trapped wave event at the Hawaiian Islands" Journal of Geophysical Research 107 (C10), 3169.

Roelvink, J.A., Wasltra, D.J., (2004). "Keeping in simple by using complex models," 6th International Conference on Hydroscience and Engineering, Advances in Hydro-Science and Engineering, Brisbane, Australia.

Roelvink, J.A., (2006). "Coastal Morphodynamic Evolution Techniques Coastal Engineering. 53, February (2006) 277-287

Stelling, G.S., (1984). "On the construction of computational methods of shallow water flow problems," Rijkswaterstaat communications, No. 35

Storlazzi, C.D., McManus, M.A., Logan, J.B. McLaughlin, B.E., (2006). "Cross-shore velocity shear, eddies and heterogeneity in water column properties over fringing coral reefs: West Maui, Hawaii," Continental Shelf Research 26 (2006) 401 –421

Sun, L.C., (1996). "The Maui algal bloom: the role of physics," In: Wiltse, W. (Ed.), Algal Blooms: Progress Report on Scientific Research. West Maui Watershed Management Project, pp. 54 –57.

Tolman, H.L. 2002. Validation of WAVEWATCH III version 1.15 for a global domain. NOAA / NWS / NCEP / OMB Technical Note Nr. 213: 33.

Tracy, B., Hanson, J., Cialone, A., Tolman, H.L., Scott, D. and Jensen, R. 2006. Hawaiian Islands Severe Wave Climate 1995-2004; 9th Waves Workshop Program. September 24-29. Victoria B.C.

U.S. Army Corps of Engineers. 2002. Shore Protection Projects. Coastal Engineering Manual: V-3-59.

Walstra, D.J.R., Roelvink, J.A., Groeneweg, J., (2000). "Calculation of wave-driven currents in a 3D mean flow model," Proc. 27th Int. Conf. on Coastal Engineering. ASCE, New York, pp. 1050– 1063.

Walstra, D.J.R., Van Rijn, L.C., Boers, M., Roelvink, J.A., (2003). "Offshore sand pits: verification and application of hydrodynamic and morphodynamic models," Proc. 5th Int. Conf. on Coastal Sediments '03. ASCE, Reston, Virginia

MAXIMUM ANNUALLY RECURRING WAVE HEIGHTS IN HAWAI´I

ABSTRACT

The goal of this study is to determine the maximum annually recurring wave height approaching Hawai´i. The motivation is scientific as well as administrative; to enhance understanding of the recurring nature of dominant swell events, as well as to inform the Hawai´i administrative process of determining the "upper reaches of the wash of the waves" (Hawai´i Revised Statutes (H.R.S.) § 205-A), which delineates the shoreline. We test three approaches to determine the maximum annually recurring wave including log-normal and extremal exceedance probability models and Generalized Extreme Value (GEV) analysis using 25 years of buoy data and long-term wave hindcasts. The annual recurring significant wave height is found to be 7.7 ± 0.28 m (25 ft ± 0.9 ft), and the top 10% and 1% wave heights during this annual swell is 9.8 ± 0.35 m (32.1 ft ± 1.15 ft) and 12.9 ± 0.47 m (42.3 ft ± 1.5 ft) respectively, for open north and northwest swell. Directional annual wave heights are also determined by applying hindcasted swell direction to observed buoy data lacking directional information.

The islands of Hawai´i lie in the midst of a large swell-generating basin, the north Pacific. Tropical storms tracking to the northwest and north of the islands produce winter swell with breaking face heights exceeding 5 m several times each year. These swell events lead to concerns over coastal erosion, coastal flooding, and water safety for the large population of ocean communities in Hawai´i. Runup generated by the largest of these waves poses a hazard to coastal development by flooding roadways, undermining structures and

causing erosion. According to Hawai´i State law (Hawai´i Revised Statutes (H.R.S.) § 205-A) the highest runup of these annual swells sets the legal position of the shoreline.

In Hawai´i, the shoreline serves as a reference line used to delineate public beach access, construction setbacks, state conservation land, submerged lands, and the border of management jurisdiction. Several states define the shoreline differently, for instance California uses the mean high water mark and Massachusetts uses the mean low water mark based on tidal water levels (not including wave setup or runup). In 1968, the State of Hawai´i changed the definition of the shoreline from the mean high water mark to the highest reach of the waves (IN RE ASHFORD). The State of Hawai´i definition of the shoreline is "the upper reaches of the wash of the waves, other than storm and seismic waves, at high tide during the season of the year in which the highest wash of the waves occurs, usually evidenced by the edge of vegetation growth, or the upper limit of debris left by the wash of the waves" (Hawai´i Revised Statutes (H.R.S.) § 205-A). In Oct. 2006, the Hawai´i Supreme Court issued a ruling (Diamond v. State of Hawai´i) that the shoreline should be established "at the highest reach of the highest wash of the waves."

The State of Hawai´i has established a coastal management system that relies on this definition of the shoreline, not only as a demarcation of public shoreline access, but also to establish a baseline for construction control and development setbacks. The discord of private landowners seeking to preserve or develop the economic value of their property and public ocean users wishing to access and preserve pristine coastal environments is responsible for continuing debate over shoreline laws. Resolving the annually recurring maximum wave height around the islands would improve the scientific basis to understanding the shoreline definition, since this line is set by the upper limit of wave runup

resulting from the largest or set of largest annually recurring waves (under optimal run-up conditions).

Local consulting engineers as part of their respective design projects on the coast are required to describe the regional and local wave climate. This analysis typically consists of specifying the largest characteristic ranges and scatter tables or rose diagrams of wave height, period and direction of the dominant swell regime for the area of interest. Such engineering reports (e.g. Noda and Associates 1991, Bodge & Sullivan 1999, Bodge 2000) do not give detailed statistical analyses of the recurring nature of swells in Hawai´i.

To provide a comprehensive analysis, we wish to resolve the annually recurring maximum wave based on the best records and state-of-the-art methods. The determination of the annually recurring wave height is also the first step to ensuring a sound scientific basis for policy-based decision-making involved in the determination of the shoreline as defined by H.R.S. § 205-A.

PREVIOUS WORK

The seasonal wave cycle in Hawai´i has been explored in several different publications. Moberly and Chamberlain (1964) outlined the wave cycle in terms of four swell regimes: north Pacific swell, northeast trade wind waves, Kona storm waves and southern swell. We have added a wave rose to their original graphic depicting annual swell heights and directions (**Figure 24**).

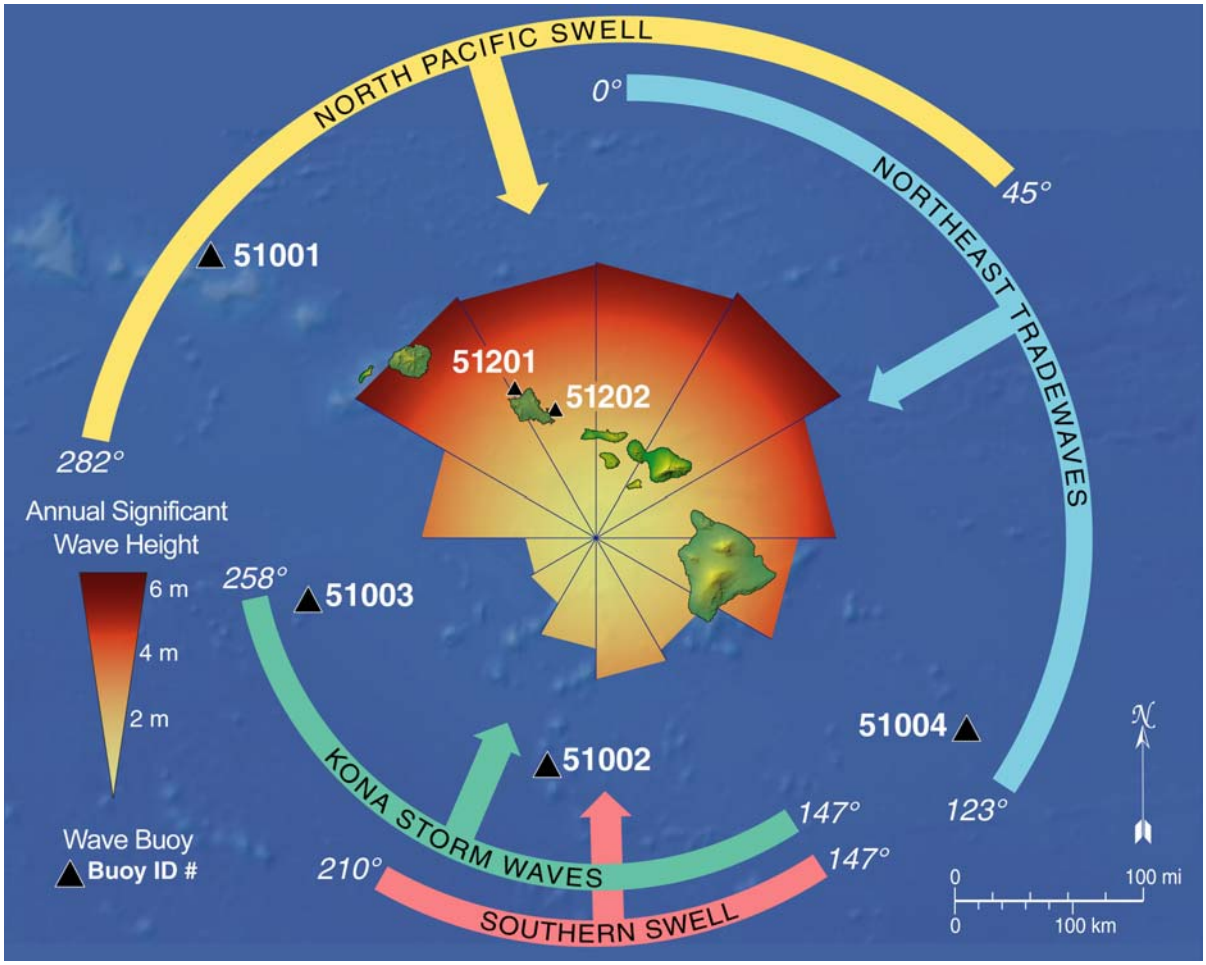

Figure 24 - Hawaii dominant swell regimes after Moberly and Chamberlain (1964), and wave monitoring buoy locations.

The seasonal wave cycle in Hawai´i is characterized by large north Pacific swell and decreased trade wind waves dominating in winter months and southern swell accompanied by increasing trade wind waves dominating in summer months. However, large-scale oceanic and atmospheric phenomena including El Niño Southern Oscillation (ENSO) and Pacific Decadal Oscillation (PDO) are thought to control the number and extent of extreme swell events (Seymour et al. 1984, Caldwell 1992, Inman and Jenkins 1997, Seymore 1998, Allan and Komar 2000, Wang and Swail 2001). Extreme wave events have been argued to

control processes such as coral development (Dollar and Tribble 1993, Rooney et al. 2004) and beach morphology (Moberly and Chamberlain 1964, Ruggiero et al. 1997, Storlazzi and Griggs 2000).

While there are several factors that contribute to annual variability in maximum wave height in Hawai´i including the ENSO and PDO cycles, the legal importance of the annually recurring wave height requires its clarification. Ruggiero et al. (1997) evaluated extreme runup using empirical equations as a means of calculating frequency of dune impact. This empirical approach or a more robust process-based numerical modeling approach could similarly be used to evaluate the extent of extreme runup in Hawaii based on the annual maximum wave height. This study could provide boundary conditions for a more sophisticated wave transformation and runup model for identification of the shoreline in Hawai'i for a particular location.

MATERIALS AND METHODS

To determine the annually recurring maximum wave height we use the record of wave buoys from the National Oceanic and Atmospheric Administration (NOAA) National Data Buoy Center (NDBC) and WaveWatch III (WWIII) model hindcasts from the Coastal and Hydraulics Laboratory's (CHL) Wave Information Studies (WIS) program (Vicksburg, Miss.).

Hourly reports of significant wave height (average of the largest 1/3 of wave heights, H_s) and other meteorological information from monitoring buoys are available from NOAA's NDBC website (http://www.ndbc.noaa.gov/Maps/Hawaii.shtml). Based on the observation that wave heights follow a Rayleigh distribution we can use the significant wave height to estimate other statistics of a swell, such as the mean wave height or the top 10%

wave height, based on the significant wave height. These buoys have an instrument precision of 0.2 m, which result in small errors (less than 5% for all waves above 4 m).

Our focus concerns buoy 51001 (buoy 1), which is located 170 nautical miles northwest of the island of Kauai and is moored at a depth of 3.25 km. The buoy has recorded 25 years of wave height and period data, since 1981.

Buoy 1 is ideally located to record north and northwest Pacific swell without interference from neighboring islands. Only recently has buoy 1 been able to record swell direction. Thus the time-series recorded in the majority of buoy 1 and all of the remaining buoys lack swell direction. The lack of observations of wave direction means that any analysis of open north and northwest swell is limited to buoy 1 as all the remaining buoys are significantly affected by island blockage, however hindcasts using Wave Watch III can be used to recover directional information.

Long-term statistical analysis is applied to the simple case of the 1-year recurring significant swell height. Statistics of extremes can usually be extrapolated to approximately 3 times the length of the time-series. As we are primarily interested in the annually recurring maximum wave height, our 25 year time-series is more than adequate to resolve this value. Long-term statistical models are typically applied to long return period events such as the 50-100 year events; such methods were originally developed to define stream flood heights or return periods from discharge records (Gumbel 1941). Although typically applied to long return periods, they can also be applied for short and intermediate return periods. The following procedure was used to construct our long-term statistical model:

1. Large swell events (n per year) from the buoy record are assigned an exceedance probability (given below).
2. Log-normal and extremal models use linear regressions to determine the relationship between large swell events and exceedance probability (the probability that a larger swell event will occur during the return period). To corroborate this analysis Generalized Extreme Value (GEV) probability models also determine the relationship between large swell events and exceedance probability using Maximum Likelihood Estimates (MLE).
3. Methods including removing outliers and the Peak Over Threshold (van Vledder et al. 1993) method are evaluated to improve model performance.
4. These statistical models assign probabilities to a full range of swell heights and are modified to give the relationship between swell heights and return period (particularly the 1-year return period).
5. The maximum annually recurring wave height is determined from the tail of a Rayleigh distribution.

The log-normal statistical models is constructed on the assumption that maximum swell events will plot as a linear function on a horizontal logarithmic-scale of exceedance probability. Exceedance probability ($Q = 1 - p$) is given by the probability that the next swell will be greater than the sorted wave events on record as if drawing from a hat containing all the maximum swell heights and the next swell event.

Wave Height	Q = Exceedance probability = (1-p)	
$H_{s1} \rightarrow$	$\frac{N}{N+1}$	← **HIGH PROBABILITY THE NEXT SWELL WILL BE LARGER.**
$H_{s2} \rightarrow$	$\frac{N-1}{N+1}$	
$H_{s3} \rightarrow$	$\frac{N-2}{N+1}$	
⋮	⋮	
$H_{sN} \rightarrow$	$\frac{1}{N+1}$	← **LOW PROBABILITY THE NEXT SWELL WILL BE LARGER.**

In this procedure, H_{s1} is the smallest significant wave height, H_{sN} is the largest significant wave height and N is the total number of waves in the analysis. Selecting different numbers of events (n) per year, such as the single maximum significant wave height each year or the top 25 significant wave heights, can yield different results as discussed later.

Our long-term statistical analyses have been performed using the significant wave height. To determine the maximum wave height that occurs with a given significant wave height requires further statistical analysis on a probability distribution of random waves.

RESULTS

Our results fall into two categories: results using the log-normal and extremal exceedance probability models and results using the generalized extreme value models.

Log-normal and Extremal Models

The log-normal model of exceedance probability vs. wave height, as seen in **Figure 25**, is quite linear on a log (x-axis) - linear (y-axis) scale.

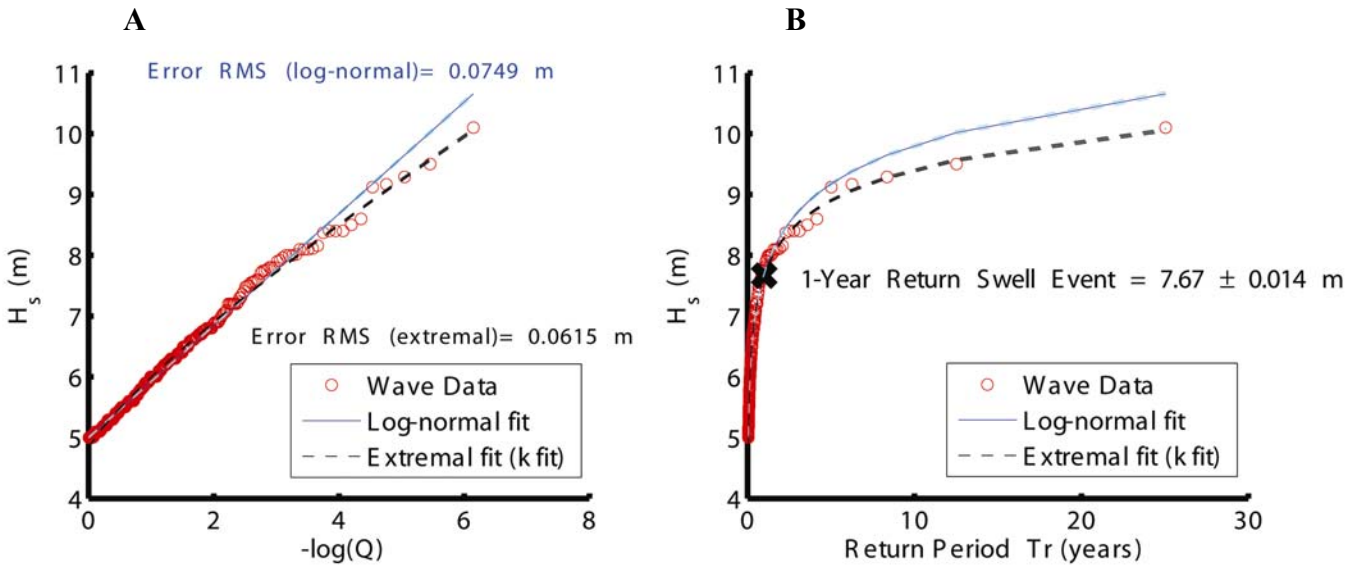

Figure 25 - Log-normal and extremal probability models for the top 70 largest wave height events per year recorded by buoy 1. In these models the largest event (a 12.3 m significant wave height) outlier has been removed and the peak over threshold method is used with a threshold of 5 m.

Figure 25-A shows a log-normal model of the data, with the following equation:

$$H_s = A[-\log Q] + B$$

Where A and B are regression coefficients.

An extremal model of the same data is shown in **Figure 25-A** and uses the following equation, which differs from the log-normal model by the $1/k$ exponent term (below), which serves to limit the occurrence of extremely large events (when k > 1) and give a better fit:

$$H_s = A[-\log Q]^{1/k} + B$$

Figure 25-B shows the same data in terms of significant wave height vs. return period instead of exceedance probability. This allows determination of the annually recurring significant wave height. The relationship between the exceedance probability (Q) and the return period (T_R) is:

$$T_R = \frac{r.i.}{Q}$$

where *r.i.* is the recurrence interval.

The return period is simply the recurrence interval, *r.i.* , (1/70 yrs since we are taking the top 70 events each year) divided by the exceedance probability (*Q*). In this case 70 events is the smallest number of recorded wave heights in a year of buoy data, as the buoy was down for the majority of 1983 due to maintenance issues.

The 1-year return period is given in **Figure 25-B** as 7.67 ± 0.014 m. The confidence levels, CI, shown in **Figure 25-A,B** are given by the typical confidence interval equations for a linear regression:

$$CI = t_{N-2,1-\frac{\alpha}{2}}(SE)\sqrt{\frac{1}{N} + \frac{(x-\mu)^2}{\sum(x-\mu)^2}}$$

where *t* is given by the student-t statistic, α is the significance level, μ is the mean, and SE is the standard error given by the equation, $SE = \sqrt{\frac{1}{N-2}\sum(y-\hat{y})^2}$.

This 1-year return swell event has an annual return probability percentage based on the recurrence interval of the time-series given by the equation:

$$E = 1 - \left(1 - \frac{r.i.}{T_R}\right)^{\left(\frac{L}{r.i.}\right)}$$

Where, *E* is the probability we will encounter the event (= 64% for the following conditions), *r.i.* is the recurrence interval (1/70 yrs), T_R is the return period (1 year), and *L* is the lifespan (1 year). According to the buoy 1 time-series, significant wave heights exceeding 7.7 m have occurred in 16 of the 25 years on record, i.e. 68 % of the time, which is consistent with the encounter probability of 64% calculated above.

Log-normal models tend to over-predict large events because physical processes exert natural limitations on event magnitude that are not accounted for in the model. For instance, flood height is limited by the rainfall amount, wave height is limited by energy dissipation, and hurricane intensity is limited by heat transfer to fuel propagation. Thus, extreme events (long return period events) are often not best fit with a log-normal relationship, and other models such as the extremal model should be considered. A particular example of this concerns the largest significant wave height in the 25-year record of buoy 1: a 12.3 m event that occurred at 4:00 am on November 5th, 1988. The second largest on record is 10.1 m (1985). These are the only two events with significant wave heights exceeding 10 m and notably, the largest swell on record is more than 2 m greater than the next largest swell. In the analysis above this 12.3 event is removed. We must consider the possibility that the 12.3 m significant wave height event was an extraordinary swell, and perhaps unlikely to occur during a period of 25 years. In exceedance probability models the largest event (12.3 m) provides information about the longest return period of recorded data (25 years in this case). In reality, this 12.3 m event could very well be the 50 or 100-year swell event, and including this event over-estimates the frequency of large events in the model as well as affects the value for the annually recurring wave height. A simple procedure is to test potential over-estimation to determine the best fit *without* the outlier event and determine the expected return period of the removed outlier. Using the model above, the return period of a 12.3 m event is approximately 150 and 700 years using log-normal and extremal models respectively. Typically, forecasts longer than 3-4 times the data collection period (25 years in this case) are not realistic, and further more they are not the focus of this paper. However,

we perform such analysis to confirm our suspicion that a very large event occurred in 1988 with a recurrence interval exceeding 100 years, and justify its removal from the analysis.

Returning to the annual return period, a log-normal model would perhaps be appropriate, but for completeness we investigate the behavior of swell events using both log-normal and extremal models as well as the GEV model (below). The GEV statistical model returns very similar results to the log-normal and extremal models, which focus on our estimates of the annually recurring significant wave height.

Generalized Extreme Value (GEV) Model

The Generalized Extreme Value (GEV) distribution is applied to determine relationships between wave height and return period with particular focus on the annually recurring wave height. Introduced by Jenkinson (1955), the GEV distribution uses Gumbel (type I), Frechet (type II), and Weibull (type III) distributions for different values of the shape parameter, $\kappa = 0$, $\kappa < 0$, $\kappa > 0$ respectively. Iterative maximum-likelihood estimates (MLE) fit the observed data to find the best estimates of the shape (κ), scale (σ) and location (μ) parameters of the GEV cumulative distribution function, $F(x)$, given by:

$$F(x) = \exp\left\{-\left[1+\kappa\left(\frac{x-\mu}{\sigma}\right)\right]^{-\frac{1}{\kappa}}\right\} \qquad \text{for } \kappa \neq 0$$

$$\exp\left\{-\exp\left[-\frac{(x-\mu)}{\sigma}\right]\right\} \qquad \text{for } \kappa = 0$$

Based on given probability distributions and the return period probability equation $p_{T_R} = 1 - \frac{r.i.}{T_R}$, wave height for an arbitrary return period is found. The GEV model is more robust than the previous approach because it combines the Gumbel, Frechet, and Weibull extreme value distributions, although it yields very similar results to our log-normal and extremal analysis (**Figure 26**). The GEV analysis, being a more robust model, remains largely unaffected by the presence of the 12.3 m event.

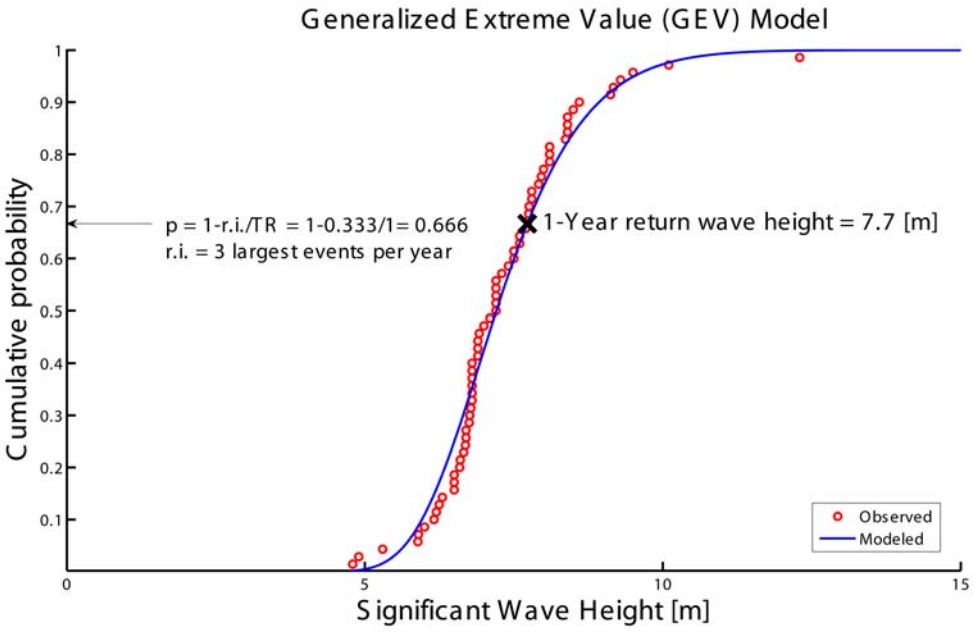

Figure 26 - The Generalized Extreme Value probability model used to determine the annually recurring significant wave height.

RECOVERING SWELL DIRECTIONALITY FROM MODEL HINDCASTS

Thus far the annually recurring wave height analysis is applicable to open north and northwest swells since no information of wave direction has been considered. By using WaveWatch III (WWIII) model hindcasts concurrent with buoy data to recover the directionality of wave heights we can determine the annually recurring maximum wave heights for a particular direction window. WWIII is an ocean-scale spectral wave model on a 0.5 degree grid which computes open swell generation and propagation based on spatial wind fields. WWIII has been well-validated using buoy and altimetry data (Tolman 2002, Baird and Associates 2005, Tracy et. al. 2006). **Figure 27** and **Table 3** below show the annually recurring maximum significant wave heights according to buoy data for extremal and GEV

models for swell direction windows of 30 degrees. Applying modeled direction to the actual buoy data may seem problematic, however it is the best option to ensure preference towards observed over modeled wave height. As you can see from **Figure 27**, observed directional annually recurring maximum significant wave heights produced by both models are similar as are results from the observed vs. modeled wave heights shown in **Table 3**.

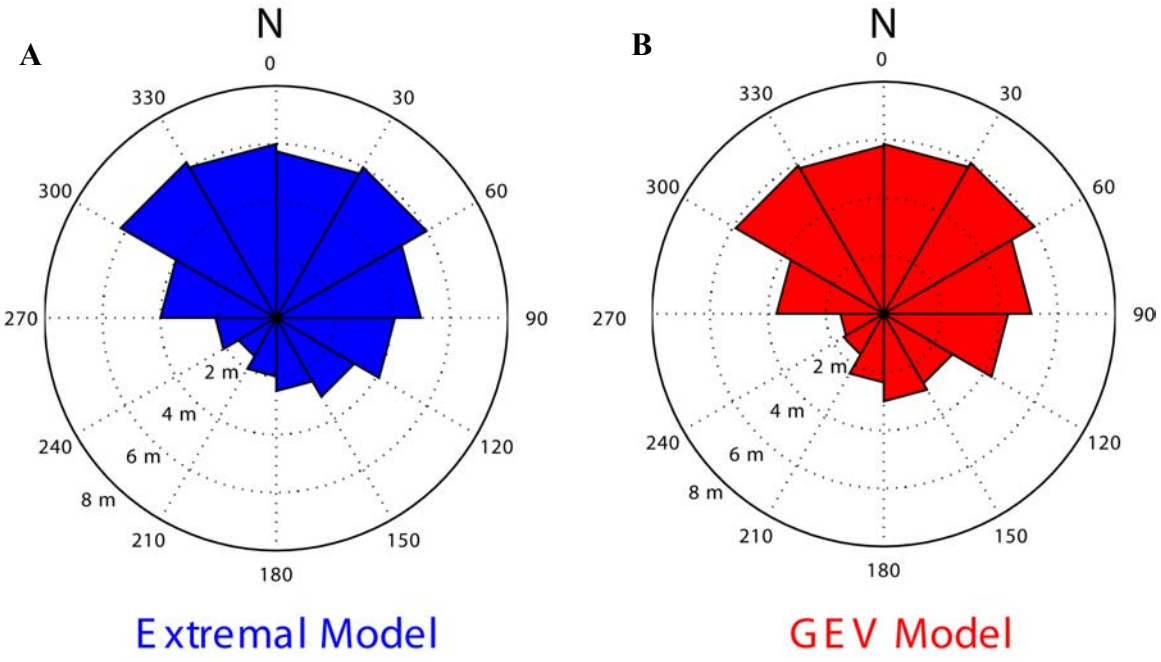

Figure 27 – The observed directional annually recurring maximum significant wave heights (H_s) given from extremal (A) and GEV (B) models.

Table 3 - The observed and modeled directional annually recurring maximum significant wave heights using extremal and GEV exceedance probability models. Wave hindcasts of Buoy 3 do not return more than one swell event per year in the southerly and westerly directional windows; hence Buoy 1 is used instead.

Window		***Source***	***Annual Hs [m] - Extremal Model***		***Annual Hs [m] - GEV Model***	
Lower	Upper		Observed	Modeled	Observed	Modeled
0	30	Buoy1	5.75	6.1	5.85	6.15
30	60	Buoy1	6	6.5	6	6.45
60	90	Buoy4	5	5.25	5.1	5.37
90	120	Buoy4	4.1	4.2	4.3	4.32
120	150	Buoy4	3.1	3.1	2.75	2.65
150	180	Buoy2	2.5	2.4	3	2.95
180	210	Buoy2	2	2.1	2.35	2.35
210	240	Buoy1	1.5	1.5	1.6	1.65
240	270	Buoy1	2.1	2.2	1.5	1.6
270	300	Buoy1	4	4.5	3.7	3.9
300	330	Buoy1	6.2	6.7	5.9	6.4
330	360	Buoy1	6	6.5	5.8	6.2

The north to northwest windowed annual significant wave heights found in this table are smaller than the previously determined value of 7.7 m because the largest events used in the analysis above do not fall into the same 30 degree windows. This limiting effect is caused by the directional variability of north swells, which typically range clockwise from 270^{o} to 90^{o} (W-E). Analysis of all northern facing swell directions (270^{o} -90^{o}) recovers this 7.7 m annual wave height. Southern swell occurs in much more narrow banded directions, typically ranging clockwise from 150 to 210 (SSE-SSW), and therefore, should be much less affected by the limiting effect of the directional variability.

SIGNIFICANT WAVE HEIGHT VS. MAXIMUM PROBABLE WAVE HEIGHT

It is important to keep in mind that 7.7 m is the annually recurring *significant wave height* or the average of the highest 1/3 of the wave heights. Each wave height data point from the buoy record used in the analysis was part of a swell train that certainly contained larger waves. The significant wave height represents the typical observational state of the ocean, not the very largest waves that occur during a swell event. To determine the largest 10% and 1% of wave heights, we assume the probability distribution of the waves follows a Rayleigh distribution, which has the following probability distribution function (pdf),

$$p(H) = \frac{2H}{H_{rms}^2} \exp\left[-\left(\frac{H}{H_{rms}} \right)^2 \right]$$

Where *p(H)* is the probability of encountering a wave of a given height, *H*, and H_{rms} is the root mean square wave height, which is equal to $H_s / \sqrt{2}$.

The assumption that random waves follow a Rayleigh distribution has been shown to be quite good for deep-water waves with a narrow-banded wave spectrum (Longuet-Higgins 1952), i.e. waves created by a single swell event rather than two converging swell events. With a given pdf, one can determine several parameters of interest, such as the average of the 10% largest waves or the maximum probable wave. Maximum probable wave, $H_{\max}$, can be solved using the following equation:

$$\int_{H_{\max}}^{\infty} p(H) dH = 1/N$$

Where *N* is the number of waves in the swell event. Solving for $H_{\max}$ yields the following equation:

$$H_{\max} = H_{rms}\sqrt{\ln N} = H_s\sqrt{\frac{1}{2}\ln N}$$

The average of the 10% largest waves is given by the following equation:

$$\text{Avg. of } H_{10\%} = \frac{\int_{H_{10\%}}^{\infty} p(H)HdH}{\int_{H_{10\%}}^{\infty} p(H)dH} \quad \text{or more generally,} \quad \text{Avg. of } H_{pct\%} = \frac{\int_{H_{pct\%}}^{\infty} p(H)HdH}{\int_{H_{pct\%}}^{\infty} p(H)dH}$$

Where $H_{10\%}$ *or* $(H_{pct\%})$ is given by the equation: $H_s\sqrt{\frac{1}{2}\ln\frac{1}{pct}}$, where *pct* is the percent of interest. By integrating the equation above, the average of the top percentages of wave heights in relation to the significant wave height are shown on **Figure 28**.

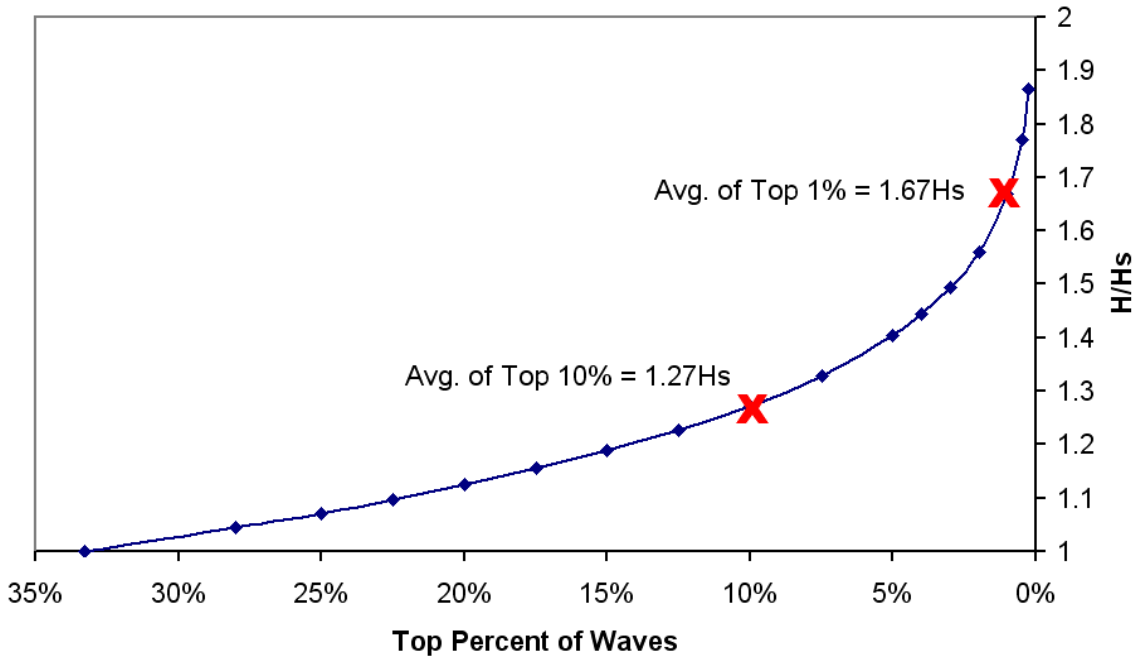

Figure 28 - Top percent of waves vs. relation to significant wave height (H_s)

Consistently, according to the Coastal Engineering Manual (CEM 2002) the average of the largest 10% and 1% of wave heights in a swell event are given by the following:

$$H_{10\%\ \text{highest}} = 1.27 H_s = 9.8 \text{ m}$$
$$H_{1\%\ \text{highest}} = 1.67 H_s = 12.9 \text{ m}$$
$$H_{\max} = 1.86 H_s = 14.3 \text{ m}$$

This analysis, for H_{max}, is based on 1000 waves and represents wave conditions that would occur for a peak swell duration of around 4.44 hours assuming the typical wave period is 16 s.

DISCUSSION

The number of maximum swell events (3 per year vs. some other number) used in the exceedance probability model influences the determination of the annually recurring significant wave height. This motivates a sensitivity test to determine the optimal number of events to use. Notably, as more events are selected per year the annual recurring wave height is higher for the log-normal and extremal models and lower for the GEV model after a peak at about 10 events per year. However when large numbers of events are selected ($N > 10$) the return wave height prediction for the log-normal and extremal models begins to stabilize **Figure 29**.

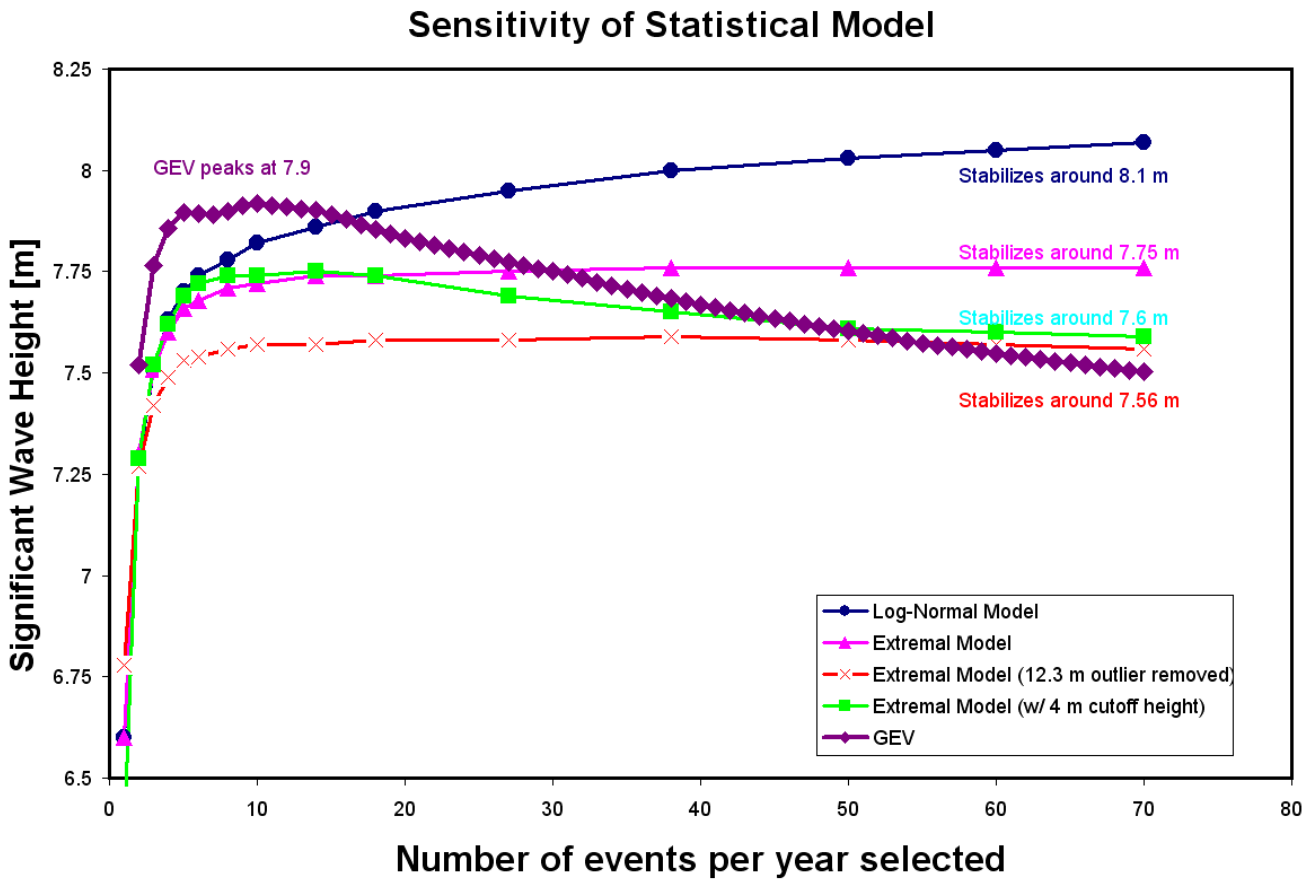

Figure 29 - Sensitivity of models to number of largest events selected per year.

This increasing annual recurring wave height result for the log-normal and extremal models is due to the trend that as more events are selected per year, the data become saturated with lower swell events, which tend to dominate the behavior of the regression. Because a majority of data points behave with a return period of less than one year, the log-normal model predominantly captures the behavior of the frequency of short return period events at the expense of long period data. This can be seen in **Figure 30** as the log-normal fit is quite good for short return period data and problematic for long return period data.

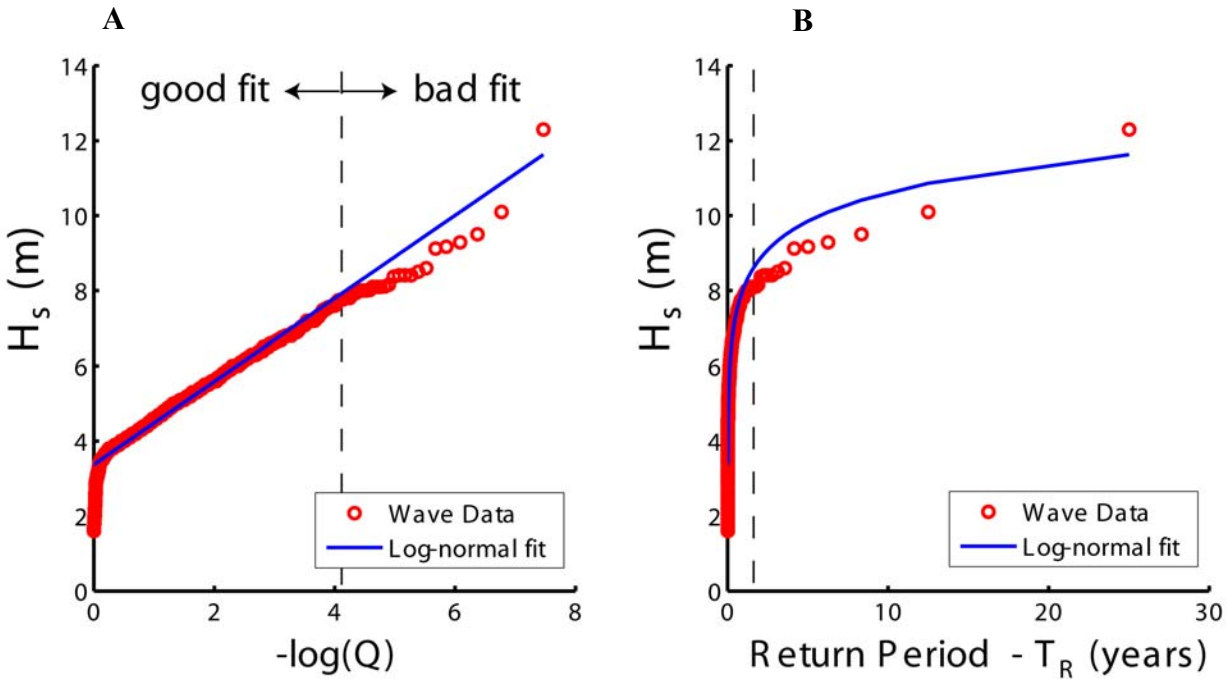

Figure 30 – When a large number of events is used in analysis, the log-normal model is fit strongly the high frequency events (which represent the bulk of the data) at the expense of the extreme events.

As seen in **Figure 30-A** a large number of short return period (high exceedance probability) data points force the slope of the log-normal fit to be higher than it would be for

long return period data points, which seem to have a lower slope. This suggests that the inherent behavior or occurrence of short return period events differ from long return period events and thus the entire dataset is not appropriately represented by a log-linear model.

In dealing with estimates of the annually recurring significant wave height, it is somewhat unrealistic to give a confidence level on the order of centimeters when dealing with waves exceeding 7 meters, although by this analysis it may be statistically acceptable to do so. Rather, we make a recommendation that accounts for the variability in using different numbers of events selected each year which typically ranges ± 0.2 m and the instrument precision which is also ± 0.2 m. Summing the error in quadrature gives a confidence level of 0.28 m still represents a very narrow band of about 3.5% of the wave height.

Thus our recommendation for the annually recurring significant wave height in Hawai´i is 7.7 ± 0.28 m (25 ft ± 0.9 ft), and the top 10% and 1% wave heights during this annual swell is 9.8 ± 0.35 m (32.1 ft ± 1.15 ft) and 12.9 ± 0.47 m (42.3 ft ± 1.5 ft) respectively. For good measure we also multiply the confidence level by the coefficient given in **Figure 28**, so that the confidence levels represent the same percentage of the final value. The difference between selecting the annually recurring significant wave height as 7.5 or 7.7 or somewhere in between is fairly trivial, especially for engineering calculations as the difference between selecting one or the other results in a maximum difference of only 3.5%.

It is important to note that this analysis considers only deep-water wave heights, which are not the same as wave heights near the shoreline. There are several physical processes that can cause deep-water wave heights to increase or decrease when propagating into shallower water such as shoaling, refraction, diffraction and non-linear interactions. There are a number of theories and methods that are used to model the transformation from

deep-water wave heights to nearshore wave heights including linear wave theory, spectral and phase-resolving wave models, and empirical equations. Caldwell (2005) has applied this approach for predicting the observed breaking wave height at Waimea Bay, Hawai´i, from the deep-water wave height recorded in buoy 1.

It is also important to keep in mind that H_{max} represents the single largest wave that would occur during a swell event, and perhaps the 10% or 1% highest wave conditions (depending on the acceptable risk tolerance) would be more representative of all of the largest waves in a swell event. Another benefit of using the top 10% or 1% of wave heights is that information about the number of waves in a particular swell is not required. The analysis performed in **Figure 28** has no input on the number of waves in a swell event; only the maximum probable wave requires the number of waves as input. These values should be considered the maximum annually recurring wave height for open north and northwest facing shores such as Kauai and Oahu where swell is directly incident to the shoreline and blocking from neighboring islands is minimized. For shorelines not directly exposed to north and northwest swell the annually recurring maximum wave height may be evaluated using **Figure 27** and the relationship of H_s to H_{max}.

FUTURE WORK

The determination of the maximum annually recurring wave height is just the first step in a process of formulating a sound scientific basis to evaluate the physical processes involved in wave runup. The next step in the process involves propagation of this deep-water wave into the nearshore, and resolving the spatial variability of wave heights due to shoaling, refraction, diffraction, convergence, divergence, non-linear interactions and breaking. The spatial and physical properties of nearshore waves can be determined through modeling or

empirical approaches. Finally, to evaluate runup, these near-shore wave properties can be used as boundary conditions in a runup model, and observations of runup should be recorded during wave events with deep-water wave heights around the annually recurring maximum level.

ACKNOWLEDGEMENTS

This paper is funded by a grant/cooperative agreement from the National Oceanic and Atmospheric Administration, Project # R/EP-26, which is sponsored by the University of Hawaii Sea Grant College Program, SOEST, under Institutional Grant No. NA05OAR4171048 from NOAA Office of Sea Grant, Department of Commerce. The views expressed herein are those of the author(s) and do not necessarily reflect the views of NOAA or any of its subagencies. UNIHI-SEAGRANT- JC-06-17.

REFERENCES

Allan, J., and Komar, P. 2000. Are ocean wave heights increasing in the eastern North Pacific? *Eos* 81: 561–567.

Baird and Associates. 2005. Pacific Ocean Wave Information Study Validation of Wave Model: Results Against Satellite Altimeter Data. Prepared for U.S. Army Corps of Engineers Engineering Research and Development Center

Bodge, K. R. 2000. Independent evaluation study of proposed Kuhio beach improvements, Prepared for State of Hawaii, Department of Land and Natural Resources.

Bodge, K. R., and Sullivan, S. 1999. Hawaii Pilot Beach Restoration Project: Coastal engineering investigation, Prepared for State of Hawaii, Department of Land and Natural Resources.

Caldwell, P. 1992. Surfing the El Niño. *Mariners Weather Log* 36: 60–64.

Dollar, S. J. and Tribble, G.W. 1993. Recurrent storm disturbance and recovery: a long-term study of coral communities in Hawaii. *Coral Reefs*, 12, 223–233.

Gumbel, E. J. 1941. The Return Period of Flood Flows. *Annals of Math. Stat*. 12: 163-190.

Jenkinson, A. F. 1955. The frequency distribution of the annual maximum (or minimum) values of meteorological elements, *Q. J. R. Meteorol. Soc*., 81: 158–171.

Longuet-Higgins, M. S. 1952. On the Statistical Distribution of the Wave Heights of Sea Waves. Jour. *Marine Res.* 11: 245-266.

Moberly, R. and Chamberlain, T. 1964. Hawaiian Beach Systems. Hawaii Institute of Geophysics Report 64-2, University of Hawaii.

Noda, E.K. and associates. 1991. Wave Measurement Program: Offshore Waikiki Beach, Prepared for State of Hawaii, Department of Land and Natural Resources.

Inman, D. L., and Jenkins, S. A. 1997. Changing wave climate and littoral drift along the California coast. Pages 314–327 in O. T. Magoon, ed. Proceedings of the California and the World Ocean Conference ’97 Conference. American Society of Civil Engineers, San Diego.

Rooney, J. Fletcher, C.H., Grossman, E., Engels, M. and Field, M. 2004. El Niño Influence on Holocene Reef Accretion in Hawai‘i, *Pacific Science* vol. 58 :305–324.

Ruggiero, P., Kaminsky, G.M., Komar, P.D., and McDougal, W.G. 1997. "Extreme waves and coastal erosion in the Pacific Northwest, " Ocean Wave Measurements and Analysis, Proceedings of the 3rd International Symposium, Waves '97, 947-961.

Seymour, R. J. 1998. Effect of El Niños on west coast wave climate. *Shore & Beach* 66: 3–11.

Seymour, R. J., R. R. Strange III, D. R. Cayan, and Nathan. R. A. 1984. Influence of El Niños on California's wave climate. in B. L. Edge, ed. Proceedings of the 19th International Conference on Coastal Engineering. American Society of Civil Engineers, New York. 35:215–230.

Storlazzi, C.D., and Griggs, G.B. 2000. Influence of El Niño–Southern Oscillation (ENSO) events on the evolution of central California's shoreline. *GSA Bulletin*. 112: 236-249.

Tolman, H.L. 2002. Validation of WAVEWATCH III version 1.15 for a global domain. NOAA / NWS / NCEP / OMB Technical Note Nr. 213: 33.

Tracy, B., Hanson, J., Cialone, A., Tolman, H.L., Scott, D. and Jensen, R. 2006. Hawaiian Islands Severe Wave Climate 1995-2004; 9th Waves Workshop Program. September 24-29. Victoria B.C.

U.S. Army Corps of Engineers. 2002. Water Wave Mechanics. Coastal Engineering Manual: II-1-74.

Van Vledder, G., Y. Goda, P. Hawkes, E. Mansard, M.J. Martin, M. Mathiesen, E. Peltier and E. Thompson, Case studies of extreme wave analysis: a comparative analysis, Proceedings Waves 93, Ocean wave Measurement and Analysis, American society of Civil Engineers, pp. 978-992. 1993.

Wang, S. L., and Swail, V. R. 2001. Changes of extreme wave heights in Northern Hemisphere oceans and related atmospheric circulation regimes. *J. Clim.* 14: 2204–2221.